COMPARISON OF MIN6 CELL AGGREGATE FORMATION METHODS AND SHEAR RESISTANCE

by

Muzaffer Cagri Kocyigit

B.Sc., Cumhuriyet University, 2010

M.Sc., Ankara University, 2014

A THESIS SUBMITTED IN PARTIAL FULFILLMENT OF

THE REQUIREMENTS FOR THE DEGREE OF

MASTER OF APPLIED SCIENCE

in

THE FACULTY OF GRADUATE AND POSTDOCTORAL STUDIES

(Biomedical Engineering)

THE UNIVERSITY OF BRITISH COLUMBIA

(Vancouver)

December 2018

The following individuals certify that they have read, and recommend to the Faculty of Graduate and Postdoctoral Studies for acceptance, the thesis entitled:

Comparison of MIN6 Cell Aggregate Formation Methods and Shear Resistance

submitted by Muzaffer Cagri Kocyigit in partial fulfillment of the requirements for

the degree of Master of Applied Science

In Biomedical Engineering

Examining Committee:

James Piret, Chemical and Biological Engineering
Supervisor

Christian Kastrup, Biochemistry and Molecular Biology
Supervisory Committee Member

Susan Baldwin, Chemical and Biological Engineering
Additional Examiner

Abstract

Islet transplantation has the potential to cure type 1 diabetes, thereby avoiding the need for a lifetime of daily insulin injections. However, to protect the islet transplant from the recipients host immune system currently requires lifelong immunosuppression. Alginate gel microencapsulation is one of the biological envelopes being developed as a physical barrier to block rejection by the recipient immune system. When using emulsification for cell encapsulation, aggregates of cells are exposed to high shear stresses that can impact their recovery. This study has investigated the aggregation of MIN6 cells to develop a model system for insulin producing beta-cells. Two aggregation methods were investigated, either using a shaking agitation system or a static multi-well system without shaking. MIN6 cell aggregates generated by both methods were analyzed for their recovery after exposure to shear stresses. A disaggregation method was introduced to examine the cellular viability of the component cells in aggregates and the cells remained viable within aggregates. Finally, the aggregates were encapsulated using 1.5% (w/v) or 5% (w/v) alginate. The 5% alginate yielded higher encapsulation efficiencies and a more spherical structure with a narrower size distribution of capsule diameters, and so should be the more suitable choice for the further development of large-scale encapsulation production processing.

Lay Summary

Type 1 diabetes normally requires multiple daily insulin injections for the rest of life. However, in many cases, this is not enough to maintain a healthy, balanced blood glucose level. One response to this challenge has been to transplant healthy pancreatic cells to reverse diabetes. Encapsulation can be used as part of this method to protect the cells with a physical barrier that blocks rejection by the recipient immune system. The encapsulation process can expose cells to damaging shear and so this study investigated the aggregation of pancreatic cells to model islet transplantation. The responses of the generated aggregates to shear forces and different concentrations of alginate were analyzed as part of developing a more effective encapsulation process.

Preface

The research objectives and experimental design of this thesis were identified by me with the contribution of Dr. James Piret. All of the experiments were conducted by me.

The MS Excel sheets used for calculations of EDR and mean diameter of beads and capsules in Chapter 4 was programed by René Pedroza, a PhD student in the Piret Lab. Also, the required conditions for 5% (w/v) alginate bead generation was previously determined by René Pedroza, as well.

The experimental work in this thesis did not require any ethics approval and this thesis an original, unpublished study and has not been submitted for publication in peer-reviewed journals yet.

Table of Contents

List of Tables

List of Figures

List of Symbols

B	impeller height
d	impeller diameter
D	vessel diameter
D[4,3]	volume moment mean diameter
H	liquid height
m	mass
N	agitation rate
n_b	impeller bla$_d$es
N_p	impeller power number
V	volume
$\bar{\varepsilon}$	mean energy dissipation rate
μ	viscosity
ρ	density
θ	impeller blade angel
ϑ	kinetic viscosity

List of Abbreviations

DAMPs	damage associated molecular patterns
DMEM	Dulbecco's modified Eagle's medium
EDR	mean energy dissipation rate
FBS	fetal bovine serum
HC	hyperplastic islet derived cell line
HIT	hamster pancreatic cell line
INS-1	insulinoma cell line
IQR	inter quartile range
MIN6	the transgenic mice derived C57BL/6 insulinoma cell line
MOPS	(3-(N-morpholino)propanesulfoic acid)
PAMPs	pathogen associated molecular patterns
PEG	polyethylene glycol
PRRs	pathogen recognition receptors
PVPON	poly(N-vinylpyrrolidone)
RIN	red insulinoma cell line
SEM	standard error of mean
T1D	type 1 diabetes
T2D	type 2 diabetes
TA	tannic acid
TLRs	toll-like receptors

Glossary

Alginate beads: Gel beads generated by alginate encapsulation process without cells.

Alginate capsules: Beads generated by alginate encapsulation process include cells.

Beads: Spherical alginate droplets generated by emulsification and internal gelation.

Encapsulation efficiency: The final encapsulated aggregate number per volume of alginate is divided by the initial aggregate number per volume of alginate, multiplied by one hundred to obtain the % encapsulation efficiency.

Inflammatory response: Reaction of the host immune system to the transplanted cells or tissues, contributing to their rejection.

Insulinoma: A benign tumor of insulin producing beta cells.

Recovery: In this study, the aggregate number recovery after exposure to shear was divided by the initial aggregate number, and this number was multiplied by one hundred to obtain a % recovery.

Throw: The shaking amplitude of the shakers in mm.

Acknowledgements

I am greatly thankful to Dr. James Piret for his guidance, advice and support as well as his passion for science that kept me to move forward during my studies and research. I am honored to work under his supervision.

I thank to Chris Sherwood for always being a supportive lab manager. I really appreciate and am thankful to René Pedroza for all his help during my research. In addition, I would like to acknowledge the other members of the Piret lab for their support and friendship.

Special thanks are owed to my mother who always supports me and believes in me.

I received a fellowship from the Turkish Ministry of Education for my studies.

Dedication

To my parents…

Chapter 1: Introduction

Diabetes (diabetes mellitus) is a chronic disease that occurs when normal blood glucose levels (normoglycemia) are imbalanced, usually increased by either the lack of insulin secretion by pancreatic β cells, insulin dependent diabetes, or the inadequate response of the body to insulin, non-insulin dependent diabetes (International Diabetes Federation, 2017). The pancreas contributes to both endocrine and exocrine functions in human metabolism through its specialized cells, islets of Langerhans and exocrine acinar cells, respectively. While the acinar cells produce and secret the required digestive enzymes for the breakdown of carbohydrates, proteins and lipids, the endocrine role of islet of Langerhans within the energy metabolism is to balance of human blood glucose levels mainly by secretion of two major hormones, insulin and glucagon (McAndrews and Wu, 2013; Marciniak *et al.*, 2014). Insulin is secreted by β cells when the blood glucose level is high (hyperglycemia), and this stimulates the uptake of glucose by cells and the synthesis of glycogen from glucose to reduce the blood glucose levels. Glucagon, secreted by α cells when the blood glucose level is low (hypoglycemia) promotes the catabolism of glycogen to increase the blood glucose level (McAndrews and Wu, 2013).

As of 2014, an estimated more than 400 million people worldwide are affected by diabetes (WHO, 2014; Song and Roy, 2016; International Diabetes Federation, 2017), and as of 2015 in Canada 3.4 million people over the age of 20 (9.3% of the population), suffer from diabetes mellitus (Canadian Diabetes Association, n.d.). The classification and diagnosis of diabetes has been investigated and developed over many decades. Diabetes is currently

classified as mainly non-insulin dependent type 2 diabetes (T2D) for ~90 per cent of diabetes cases, or insulin dependent type 1 diabetes (T1D) for ~10 per cent of total diabetes cases (International Diabetes Federation, 2017). Type 1 diabetes is severe and produces complete insulin deficiency resulting from autoimmune destruction of insulin producing β cells in the pancreas (Wardle, 2013; Zinger and Leibowitz, 2014; Song and Roy, 2016).

The hyperglycemia condition in T2D is associated with; obesity, ageing, sedentary lifestyles or inactivity, it is characterized by either insulin deficiency or a decrease in the insulin stimulated glucose uptake (Ishihara *et al.*, 1993; Donath and Shoelson, 2011; Chatterjee, Khunti and Davies, 2017). T2D can lead to cardiovascular complications and further health issues if untreated (Donath and Shoelson, 2011; Chatterjee, Khunti and Davies, 2017). T2D can be counteracted by lifestyle changes in some cases, such as following a healthy diet, increasing the amount of physical activity and maintaining a healthy body weight. If lifestyle changes are insufficient for the treatment of hyperglycemia, then oral medication (e.g. Metformin) is used to control T2D avoiding the need for insulin injection. Nonetheless, for a significant portion of T2D patients oral medication is unable to control hyperglycemia and they must use insulin injections (International Diabetes Federation, 2017).

Type 1 diabetic patients are insulin-dependent individuals throughout their lives and must measure their glucose levels frequently, especially at meal times. The maintenance of a healthy blood glucose level is critical to avoid severe health complications (e.g. coma, cardiovascular degeneration, and retinopathy). For patients with T1D, so as to stabilize the blood glucose levels, insulin can be delivered through needle injections or subcutaneous

infusion with the aid of an insulin pump. Although this treatment can help to maintain normoglycemia, success depends on diligent glucose monitoring by patients and this is facilitated when they have an awareness of hypoglycemic conditions. The constant monitoring and correction of blood glucose levels via insulin injection act to reduce the quality of patients' lives, even in many compliant patients and it is not a cure for T1D.

Whole pancreas (cadaver) transplantation is an alternative treatment that can re-establish insulin independence, but the number of donors is very low compared to the number of patients with T1D. Furthermore, diabetic patients especially those with T1D are more likely to have cardiovascular risks and other vital complications during and after such complex transplantation surgery. In addition, the requirement for post-transplant immunosuppressive treatment may cause side-effects and add risks that make whole pancreas transplantation not worthwhile except in the most severe cases of diabetes (Johannesson *et al.*, 2015; Song and Roy, 2016). Nonetheless, the incidence and prevalence of T1D is increasing every year, increasing the importance of innovative T1D treatments, especially if this can provide a cure.

1.1 Islet Transplantation

Islet transplantation, especially since the development of the Edmonton protocol, has emerged as an alternative treatment and even possibly a cure for T1D (Shapiro *et al.*, 2000). This has been successfully used to treat diabetics for whom exogenous insulin administration therapy does not effectively re-establish normoglycemia. Islets of Langerhans, constituting 1-2% of the whole pancreas, consist of cell clusters of alpha (α), beta (β), delta (δ), pancreatic

polypeptide (PP), and epsilon (ε) cells that perform the endocrine functions of the pancreas (Brissova *et al.*, 2005; Cabrera *et al.*, 2006; Andralojc *et al.*, 2009; Marciniak *et al.*, 2014; Brereton *et al.*, 2015). The largest component of islets of Langerhans are β cells at approximately 70 per cent of islet mass. The fraction of the other cells are ~20% α cells, ~10% δ cells ~5% PP cells (Brissova *et al.*, 2005; Cabrera *et al.*, 2006; Brereton *et al.*, 2015). Insulin, glucagon, somatostatin, pancreatic polypeptide and ghrelin are respectively secreted by β cells, α cells, δ cells, PP cells and ε cells in order to regulate and maintain cellular energy metabolism and growth (Brissova *et al.*, 2005; Cabrera *et al.*, 2006; Andralojc *et al.*, 2009; McAndrews and Wu, 2013; Brereton *et al.*, 2015).

For islet transplantation by the Edmonton protocol, a pancreas obtained from a cadaveric donor is first treated with digestive enzymes and dissociated by shear forces to free the islet cell clusters. Then, the islet cells are purified from the exocrine cells using density differences, and finally infused into the hepatic portal vein for implantation in the liver (Robertson, 2004). Islet transplantation represents a far less-invasive approach compared to whole organ transplantation and has been investigated since the first trial transplanting pancreas extracts was reported in 1894 (Robertson, 2004). However, it was not until the development of the Edmonton protocol that this approach was successful (Shapiro *et al.*, 2000, 2006). This approach introduced many innovations to the conventional method of islet transplantation including the use of a glucocorticoid-free (steroid free) immunosuppressive regimen (Shapiro *et al.*, 2000; Robertson, 2004; Bassi and Fiorina, 2011). However, only approximately 40 per cent of the islet transplant patients were able to maintain insulin independency after one year and less than 10 percent 5 years post-transplantation (Ryan *et*

al., 2005; Shapiro *et al.*, 2006). Although the limited source of β cells has been another major hurdle for islet transplantation, the increasing availability of porcine or human stem cell derived β cells has the potential to be a cost effective methods to increase the cell supply for transplantation (Kieffer *et al.*, 2018). Although these sources of β cells could increase the availability of cells to treat diabetes, there remains the need to immunosuppress the recipient host immune system against these transplanted cells (Langlois *et al.*, 2009; Kizilel *et al.*, 2010; Murua *et al.*, 2011; Jung *et al.*, 2012; Song and Roy, 2016).

1.2 Immunoprotection of Transplanted Islet Cells (Encapsulation)

Lifelong immunosuppression exposes transplant recipients to toxicity as well as increased risk of infections and malignancies (Scharp and Marchetti, 2014). The treatment of these conditions adds considerably to health care systems costs (Wallner *et al.*, 2018). Thus, many studies have focused on the development of an encapsulation method for transplanted cells to reduce or eliminate the need for immunosuppression. For islet transplantation, encapsulation supplies a physical semipermeable barrier that allows the diffusion of insulin, oxygen as well as nutrients and waste products while blocking immune cells and other transplant damaging inflammatory responses. Ideally, without the need for immunosuppressive drugs, encapsulated cells should maintain normoglycemia by the natural mechanism of insulin function (Desai and Shea, 2017). The methods of islet encapsulation can be divided into three categories based on their surface area to volume ratio and diffusion distance: macroencapsulation, microencapsulation, and conformal coating, *i.e.*, a thin covering (Scharp and Marchetti, 2014; Song and Roy, 2016).

1.2.1 Microencapsulation

Microencapsulation aims to encapsulate a single or a few islets (~150 μm) inside a normally spherical, semipermeable membrane (Figure 1.1). Microencapsulation to provide an immune isolated environment for transplanted β cells has been studied over 60 years, using many capsule materials, such as agarose, polylysine, polyethyleneimine, polyethylene glycol and alginate (Scharp and Marchetti, 2014; Desai and Shea, 2017). Advantages of microencapsulation over macroencapsulation include the ease of production and their high surface area-to-volume ratios for diffusion (De Vos, Hamel and Tatarkiewicz, 2002; Scharp and Marchetti, 2014; Desai and Shea, 2017).

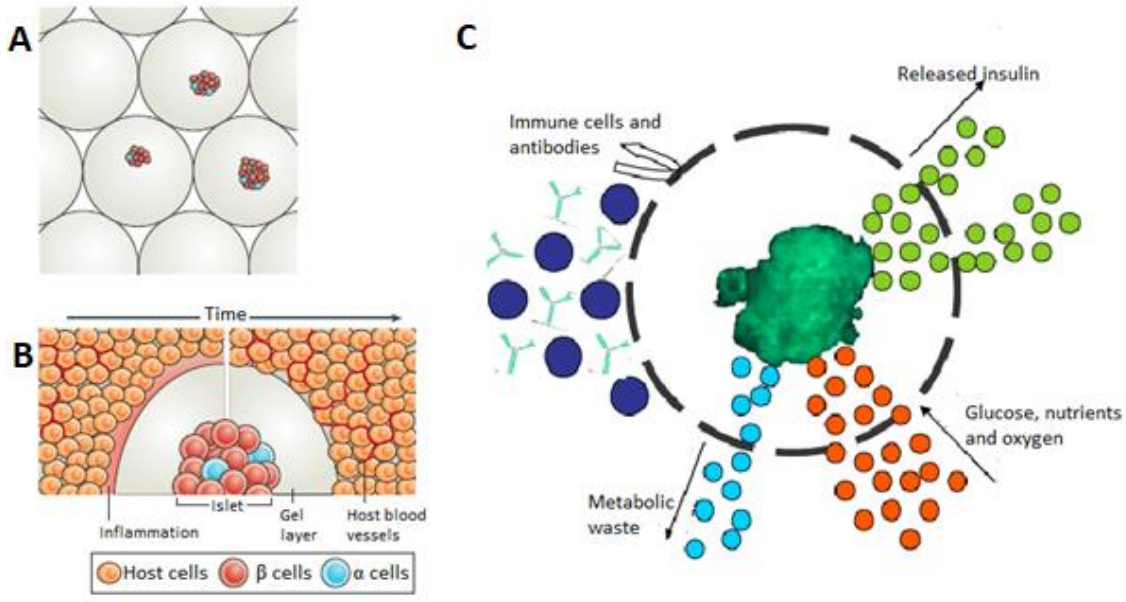

Figure 1.1 Illustration of microcapsules for islet cell transplantation
(A) Microencapsulated islets. (B) Inflammatory response of host immune system against transplanted microcapsules. (C) Semipermeable membrane allows the transport of hormones, glucose, oxygen and waste products while blocking immune cells and antibodies. (This illustration was adapted from Vaithilingam and Tuch, 2011; Desai and Shea, 2017)

This technique is also less invasive compared to macroencapsulation (De Vos, Hamel and Tatarkiewicz, 2002; Song and Roy, 2016). Because microencapsulation depends on diffusive transport (e.g. insulin and oxygen), microcapsules are usually less than 1,000 μm in diameter (Song and Roy, 2016). Many studies have reported successful immunoprotection by microencapsulation of transplanted islets; in rats (Lim and Sun, 1980), in mice (Zimmermann *et al.*, 2005), in T1D patients with xenotransplantation of neonatal porcine islet (Elliott *et al.*, 2007), or encapsulation of human islets (R Calafiore *et al.*, 2006; Riccardo Calafiore *et al.*, 2006).

1.2.2 Alginate-based capsules

Alginate is a polyanionic copolymer isolated from brown sea algae (Ertesvåg and Valla, 1998; Goh, Heng and Chan, 2012; Lee and Mooney, 2012). It has been used in the food and cosmetic industry, as well as in health care and pharmaceutical sciences. The first successful application of alginate in encapsulation technology (Lim and Sun, 1980) demonstrates its potential for cell-based therapies and transplantation (Goh, Heng and Chan, 2012; Lee and Mooney, 2012). Compared with other microencapsulation materials alginate has emerged as a more biocompatible material with fewer immunogenicity issues (de Vos *et al.*, 2006; Desai and Shea, 2017). It also has the important advantages of forming gels under nontoxic conditions and can be degelled such that the encapsulated cells can be recovered for analysis.

Alginate copolymer is naturally composed of β-D-mannuronic acid (M) and its epimer α-L-guluronic acid (G) monomer residues. These residues come together to form the copolymer

blocks in three different structures (Figure 1.2); consecutive M blocks, consecutive G blocks or sequentially altering MG blocks (Ertesvåg and Valla, 1998; Goh, Heng and Chan, 2012; Lee and Mooney, 2012). Even though some studies have reported that high M content alginates have higher immunogenicity than high G alginates, others reported almost no impact on the inflammatory response from the relative M/G composition of alginates. It is clear that the purity of alginate can correlate with immunogenic issues (Lee and Mooney, 2012). For example, compared to unpurified alginate, purified alginate microencapsulated cells have prolonged survivability after transplantation and were less immunogenic (Langlois *et al.*, 2009).

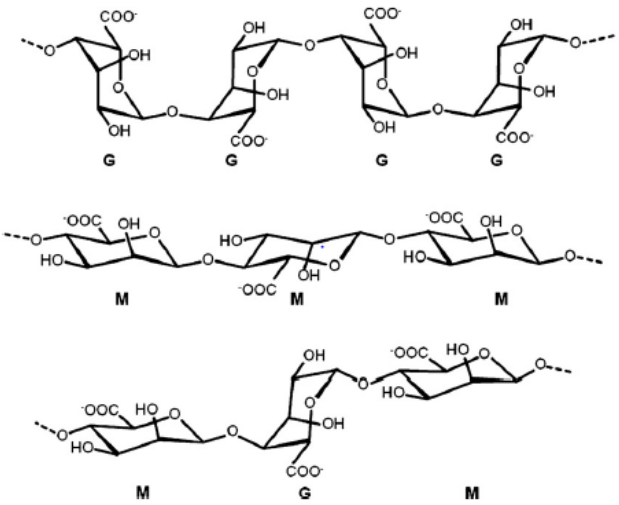

Figure 1.2 Chemical components of alginates; α-L-guluronic acid (G-blocks), β-D-mannuronic acid (M-blocks), and altered MG-blocks. (This figure is from Lee and Mooney, 2012)

Physical and chemical cross-linking methods can be classified as external gelation, internal gelation or thermal gelation (Goh, Heng and Chan, 2012; Lee and Mooney, 2012). Alginates used as hydrogels can be prepared by cation dependant cross-linking methods. For external

gelation, alginate solutions containing cells are added drop-wise to a solution containing cross-linking cations to form alginate gel beads (Goh, Heng and Chan, 2012). Emulsification-internal gelation is an alternative technique for the generation of alginate gel beads (Poncelet *et al.*, 1992). Cells are first mixed with alginate solution as well as insoluble calcium or barium salts, *e.g.*, $CaCO_3$, as cross-linking agents. This mixture is then emulsified in mineral oil by agitation to generate small droplets. Then, free Ca^{2+} ions are released by decreasing the pH with the addition of oil-soluble glacial acetic acid. With the liberation of Ca^{2+} ions, alginate gel beads are generated (Hoesli, 2010; Hoesli *et al.*, 2011; Goh, Heng and Chan, 2012). This emulsification-internal gelation method was first used to generate alginate beads for mammalian cell immobilization by Hoesli *et al.* (2010; 2011). The authors achieved faster normalization of blood glucose (normoglycemia) and more advanced graft survival in an allogeneic transplantation of diabetic mice (Hoesli *et al.*, 2012).. Hoesli *et al.* adapted this technique from the method first introduced by Poncelet *et al.* (1992) by changing the buffer system, the processing time and the bead recovery method. This emulsification-internal gelation is more scalable than extrusion and external gelation in terms of the time required for alginate bead generation, but there is a wider bead size distribution. Resolving problems of microcapsules made with the use of alginates as semipermeable membranes have focused on abolishing the inflammatory response to the transplanted islet as well as optimizing the bead diameter. Initial approaches of alginate-based microencapsulation have mainly focused on the alginate type to overcome these challenges. However, recent studies have demonstrated that the physical and chemical methods used to generate alginate microcapsules can also be important (Vaithilingam and Tuch, 2011; Desai and Shea, 2017).

1.3 Inflammatory Response to Transplanted Cells

Although alginate-based microcapsules can be biocompatible, De Vos *et al.*, 1997, showed that alginate purification improved the immunosuppressive properties of microcapsules. They compared purified alginate capsules to crude alginate capsules both of which were transplanted to the peritoneal cavity of rats. Whereas fibrotic overgrowth (a type of immune response) on the capsule surface was observed for almost all crude alginate capsules, the average overgrowth on purified alginate capsules was less than 10 percent. Even though alginate purification enhanced biocompatibility, graft viability remained limited and unrelated to alginate purification (De Vos *et al.*, 1997).

Biocompatibility is a complex phenomenon. It is not only influenced by the alginate composition or content, but also by the recipient innate immune response. Vascularization issues may also influence the inflammatory response against the transplanted capsules (de Vos *et al.*, 2006). The innate response can also be triggered by the transplanted tissue releasing or secreting molecules such as cytokines (de Vos *et al.*, 2006). Studies have shown that the inflammatory response is induced by diffusion of cytokines through the alginate membrane resulting in graft failure (De Vos *et al.*, 1999; de Vos *et al.*, 2003). Cytokines are low molecular weight proteins (less than 30 kDa) that are smaller than the alginate capsule pores whose molecular weight cut off (MWCO) can be approximately 100 kDa (de Vos *et al.*, 2006; Paredes Juarez *et al.*, 2014).

Even when using highly purified alginate as capsule material there can be activation of the innate immune response through the release of pathogen-associated molecular patterns (PAMPs). PAMPs are endotoxic impurities in alginate that may not be removed by purification (Paredes Juarez *et al.*, 2014). These alginate-derived PAMPs provoke the hosts' immune system reaction against the encapsulated β-cells. Innate receptors called pathogen-recognition receptors (PRRs) can detect these patterns. Toll-like receptors (TLRs), alongside other types of PRRs, are the receptors mostly involved in the inflammatory response against alginate-derived PAMPs. These PAMPs induce the release of cytokines or chemokines that cause cell death and eventually graft failure.

Cell death stimulates stronger responses because PRRs also detect another molecular pattern, damage-associated molecular patterns (DAMPs). These patterns are released from intracellular spaces to extracellular spaces upon cell death by necrosis or necroptosis. DAMPs in a healthy organ function to alert the other cells to stop the damage and start the healing process whereas DAMPs recognized by TLRs cause a cascade and intensification of immune system responses. Studies have shown that DAMPs are a major cause of the inflammatory response against encapsulated cells (De Vos *et al.*, 2014; Paredes Juarez *et al.*, 2014; Paredes-Juarez *et al.*, 2015). To reduce the inflammatory response and its deleterious effects, alginate used for the protective membrane should not contain PAMPs and have a smooth surface that avoids cell adhesion and fibrotic overgrowth. Also, denser alginates that decrease the membrane permeability can reduce the release of DAMPs and the entry of cell damaging cytokines into the capsules (Paredes Juarez *et al.*, 2014; Paredes-Juarez *et al.*, 2015).

1.4 Cellular Aggregate Generation

Islets of Langerhans are endocrine cell clusters that have a roughly spherical shape with a diameter of approximately 150 µm. The islet size distribution in both rats and humans vary between 20 µm to more than 400 µm (MacGregor *et al.*, 2006; Buchwald *et al.*, 2009; Huang, Ramachandran and Stehno-Bittel, 2013). When islet cells are isolated and transplanted after in vitro treatments it is important to maintain their cell-to-cell interactions to maintain their biological functions. It has been shown that aggregated cells or islets have enhanced secretory properties and greater survivability than dispersed islet cells (Hauge-Evans *et al.*, 1999). Three-dimensional (3D) aggregate structures are formed by many cell and tissue types both in vivo and in vitro. Examples include neurospheres (Youn *et al.*, 2005, 2006; Gilbertson *et al.*, 2006), embryonic bodies (Dang *et al.*, 2002; Koike, Kurosawa and Amano, 2005; Burridge *et al.*, 2007), and spheroids (Yamada and Cukierman, 2007; Verbridge, Chandler and Fischbach, 2010) . Since aggregation increases cell-to-cell interactions, aggregated β islet cells have increased insulin secretion and prolonged function after transplantation (Hauge-Evans *et al.*, 1999; Bernard, Lin and Anseth, 2012). Modulating cell aggregate sizes and the conditions for aggregate generation is a focus of this study.

1.4.1 Aggregate formation

Cell aggregation for transplantation has been studied for neural precursor cells (Gilbertson *et al.*, 2006), neural stem cells (Sen, Kallos and Behie, 2001), human pluripotent stem cells and human embryonic stem cells (Dang *et al.*, 2002; Ungrin *et al.*, 2008, 2012; Schulz *et al.*,

2012), as well as β cells and human islets (Hauge-Evans *et al.*, 1999; Bernard, Lin and Anseth, 2012; Yang *et al.*, 2013; Hilderink *et al.*, 2015). Many different aggregation methods for β cells have been employed, including aggregation in shakers and static suspension by self-assembly in non-adhesive tissue culture vessels (Bernard, Lin and Anseth, 2012).

In addition to primary β cells, pseudoislets are also used. Pseudoislets are engineered pancreatic-like cell lines that secrete insulin. These pancreatic-like cell lines have been investigated as a means to overcome the limited availability of islets for T1D treatment (Hauge-Evans *et al.*, 1999; Skelin, Rupnik and Cencic, 2010; Bernard, Lin and Anseth, 2012). These β cell lines can generally perform glucose-induced insulin secretion and some are also capable of producing glucagon and somatostatin. These cell lines also can provide useful model systems to elucidate the behaviour and functionality of β islet cells in transplantation. Naturally occurring insulinomas, generally benign tumors of β cells, were initially preferred for the generation of pancreatic-like cell lines due to their rapid proliferation. Unfortunately, both human and rat insulinomas lose their insulin secreting function in culture. Therefore, different procedures such as irradiated insulinomas or transgenic mice derived insulinomas have been used to create more stable cell lines. These cell lines include the irradiated rat insulinoma cell line (RIN), the insulinoma cell line (INS-1), the transgenic mice derived transgenic C57BL/6 mouse insulinoma cell line (MIN6), hamster pancreatic beta cells (HIT) and beta hyperplastic islet derived cells (HC) (Skelin, Rupnik and Cencic, 2010). MIN6 cells are widely used for cell aggregation studies related to islet transplantation (Hauge-Evans *et al.*, 1999; Bernard, Lin and Anseth, 2012; Yang *et al.*, 2013; Hilderink *et al.*, 2015). MIN6 cells are derived from transgenic C57BL/6 mouse insulinoma expressing the SV40 T-antigen and they are pancreatic beta-like cells that were

first reported by Miyazaki *et al.* (1990). Ishihara *et al.*, (1993) reported glucose dependent insulin secretion by MIN6 cells is similar to primary islets (Ishihara *et al.*, 1993; Skelin, Rupnik and Cencic, 2010).

Aggregation method development is essential to the generation of cell aggregates with desired features. The targeted aggregate diameter range is from 100 to 200 µm, since the average diameter of human islets is around 150 µm. To increase diffusion of oxygen to the core region of cell aggregates they should have a limited size and ideally a spherical shape. To control aggregate size MIN6 single cells have been aggregated in PEG hydrogel microwell plate (Bernard, Lin and Anseth, 2012). These plates produce aggregates in 5 days with diameters of 100, 200 or 300 µm depending on the microwell dimensions. In this study the cellular viability and insulin secretion ability of generated aggregates was compared to the single MIN6 cells. They reported that aggregated MIN6 cells have increased viability and higher glucose-stimulated insulin secretion. Aggregates with an average diameter of 100 µm have also been generated in bacterial dishes (Zhi *et al.*, 2010). The use of another low adherance dish (Kelly *et al.*, 2010) was reported suitable for the aggregate formation with an enhanced insulin secretion. Several culture plates were compared in one study (Yang *et al.*, 2013) including tissue culture treated polystyrene dishes, non-treated dishes, type IV collagen coated dishes, Lipidure dishes and ultralow attachment culture dishes. These were seeded with single MIN6 cells and it was shown that the growth substrate has an impact on aggregate function. All the aggregates generated in this study had superior characteristics compared to single cells and aggregates generated with the type IV collagen and Lipidure dishes exhibits higher cell viability and glucose stimulated insulin secretion compared to the other surfaces. Another non-adherent agarose based microwell platform study was conducted

for the formation of reproducible and controlled MIN6 cells and human islet cell aggregates (Hilderink *et al.*, 2015). This static microwell platform allowed the controlled generation of both human islet cell aggregates and MIN6 aggregates with diameters of 100-150 µm. All these studies aimed to obtain reproducible and controllable cellular aggregation models for in vivo and/or in vitro studies of islet transplantation for T1D treatment.

1.4.2 Effect of shear stress on aggregates

The encapsulation process includes shear exposure and these forces can break up aggregates into single cells. Thus, aggregates that are used for encapsulation need to be shear resistant. One of the ways to describe external shear stress is based on estimating the energy dissipation rate (EDR). This has been used to quantify cell damage on biological cultures (Gregoriades *et al.*, 2000; Mollet *et al.*, 2004). It is given as power per unit volume (W/m^3) and takes into account hydrodynamic forces in bioprocessing and culture vessel geometries (Shenkman *et al.*, 2009).

1.5 Research Objectives

The goal of this study was to investigate MIN6 cell aggregation and test the aggregate stability when they are exposed to shear. The specific aims were to:

1. Develop scalable methods to aggregate MIN6 cells as a system to simulate islet cells.
2. Develop a reliable MIN6 disaggregation method.
3. Examine the stability of MIN6 aggregates as a function of shear forces.

Chapter 2: Materials and Methods

2.1 Cell Culture

2.1.1 MIN6 cell line

MIN6 pancreatic β-like cells, first introduced by Miyazaki *et al.* (1990), were cultured in DMEM (Dulbecco's Modified Eagle Medium, with phenol red, Gibco) supplemented with 10% FBS (Fetal Bovine Serum, Gibco), 4 mM glutamine (Gibco). This medium is referred to as "complete DMEM" and was used for all processes when medium was required unless otherwise indicated. The adherent cell cultures were kept at 37℃ and 5% CO_2 in a humidified incubator, grown on tissue culture treated T-flasks (Sarstedt, T75) with a 5×10^4cells/cm^2 inoculum. Either Trypsin (Trypsin-EDTA, 0.05%, Gibco) or TrypLE (TrypLE express, Gibco) were used as the disassociation agent.

2.2 Emulsification and Internal Gelation

The emulsification and internal gelation process was previously introduced in the lab (Hoesli, 2010; Hoesli *et al.*, 2011) and adapted from Poncelet *et al.* (1992). Alginate beads and bead encapsulated aggregates were generated in an agitated spinner flask (Figure 2.1). The detailed methods are below.

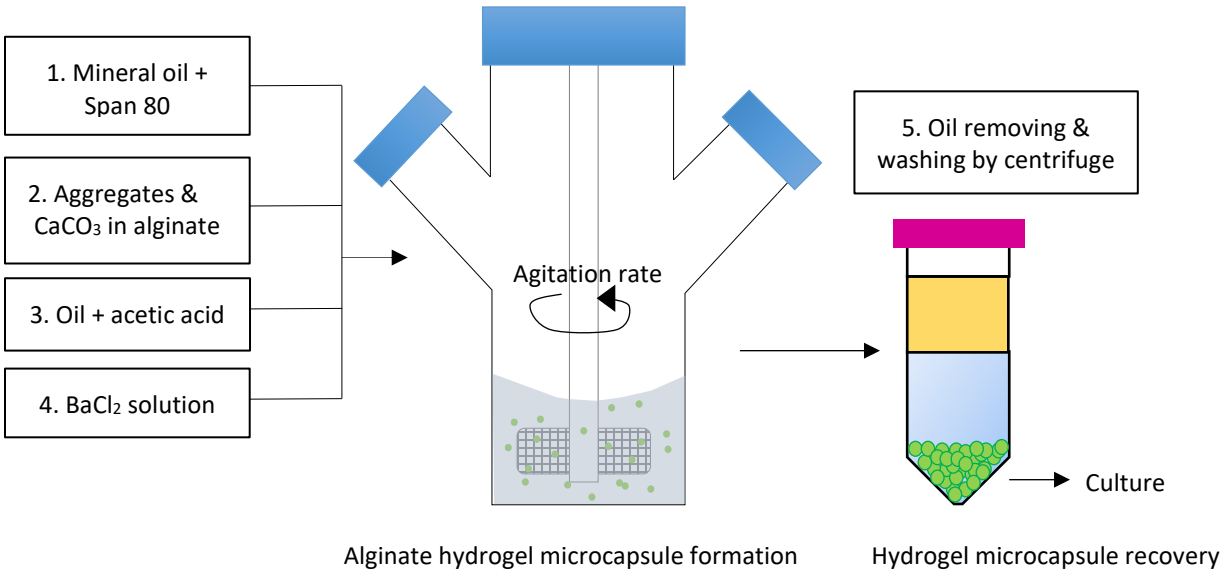

Figure 2.1 Schematic illustration of emulsification and internal gelation.

2.2.1 $CaCO_3$ solution

A stock of 0.5 M $CaCO_3$ solution was prepared by mixing 0.5 g of $CaCO_3$ in 10 mL process buffer solution (60 mM MOPS, 127 mM NaCl at pH 7.6). A working solution of 0.05 M $CaCO_3$ was prepared from a 10 times dilution of 0.5 M $CaCO_3$ stock solution in the process buffer. These solutions were stored at 4℃ after they were sterilized by autoclaving for 40 minutes at 121℃ and 90 kPa.

2.2.2 Mineral and acidified oil

The mineral oil (Fisher Chemical, Mineral oil-Light, cat. no. O121) was sterilized by filtering with a 500 mL Stericup® disposable vacuum filtration unit (Millipore Express® PLUS. 0.22 µm PES, cat. no. S2GPT05RE) under aseptic conditions, and stored at room temperature.

Acidified oil was freshly prepared before each emulsification/encapsulation process by mixing one volume of glacial acetic acid and 250 volumes of sterilized mineral oil and vortexed for at least one minute.

2.2.3 Neutralization buffer and curing solution

The neutralization buffer was a mixture of one volume culture medium (complete DMEM) and 9 volumes of process buffer. The curing solution consisted of one volume process buffer and 19 volumes of barium concentrate, composed of 60 mM MOPS, 127 mM NaCl, 1 mM $BaCl_2$ at pH 7.4. The barium concentrate and process buffer solutions were sterilized by autoclave for 40 minutes at 121℃ and 90 kPa.

2.2.4 Alginate Solution

The alginate powder (Sigma-Aldrich, Alginic acid sodium salt, cat. no. A2033, stored in a desiccator at 4℃) was dissolved in alginate buffer, consisting of 60 mM MOPS and 42 mM NaCl at pH 7.6. Alginate (11.66 g) was added to 200 mL of this alginate buffer to obtain a 5.83% w/v final alginate concentration and stirred until the alginate powder was dispersed within the alginate buffer. The alginate solution was then autoclaved at 121℃, 90 kPa for 40 minutes sterilization and to complete the dissolution of the alginate powder. Similarly, the alginate solution with 1.75% w/v final concentration was prepared by dissolving 3.5 g of alginate in 200 mL alginate buffer. Both alginate stock solutions were stored at 4℃ and warmed to room temperature prior to the emulsification and encapsulation process.

2.2.5 Emulsification and internal gelation method

1.8 mL of 5.83% (w/v) alginate solution, 0.2 mL of aggregates suspended in medium, 0.1 mL of 0.5 M $CaCO_3$, and 1.8 mL of 1.75% (w/v) alginate solution, 0.2 mL of aggregates suspended in medium, 0.1 mL of 0.05 M $CaCO_3$ were mixed as explained next, to generate 5% (w/v) and 1.5% (w/v) alginate capsules, respectively. Sterile syringes were used to prepare the alginate-aggregate mixtures (BD 309609). Using a 1 mL syringe 0.9 mL alginate solution was transferred to an outlet-capped 10 mL syringe (BD 309604), followed by the addition of 0.1 mL $CaCO_3$ as a cross-linker agent, then another 0.9 mL of alginate solution was transferred into the same 10 mL syringe and the solution was mixed 10 times using a sterile spatula. This 1.9 mL alginate-$CaCO_3$ mixture and 0.2 mL aggregate stock solution were transferred dropwise to another capped 10 mL syringe. The final alginate-$CaCO_3$ and cell aggregates were mixed by twisting and pushing and pulling the plunger of the syringe back and forth 15 times. This alginate-aggregate mixture was added into mineral oil and emulsified into smaller droplets at the selected agitation rate for 3 minutes, followed by addition of the acidified oil and agitated at the same rate for another 3 minutes. After acidification the neutralization buffer was added and stirred for 1 minute more. Finally, curing solution was added into the spinner flask and the agitation rate decreased to 120 rpm and run for another 10 minutes. The alginate capsules were recovered in 50 mL conical base tubes within the water phase by 200 g centrifugal oil/water phase separation.

2.3 Aggregate Formation

Several different aggregate formation techniques and process parameters were tested and new approaches developed to improve aggregate generation. External shear forces were initially used to generate MIN6 cell aggregates with agitation in petri dishes, well plates or shaking culture tubes. Among these vessels, shake tubes generated the most spherical and uniform aggregate structures. The formation of aggregates in 50 mL shake culture tubes was then tested at 150, 200, 225 and 300 rpm agitation rates using orbital (Heidolph Rotamax 120, 20 mm throw) or Kuhner (Kuhner Shaker X, Lab – Term LT-X, 50 mm throw) shakers. Furthermore, the effect of different cell input concentrations on aggregate generation was investigated.

Static cell aggregation was performed using AggreWell 6 and 24 well plates (AggreWell^{TM} 400, Stemcell Technologies, cat. no. 34411&34421). Each well contains a series of microwells that are 400 µm in diameter and have an inverted pyramid shape (Figure 3.7). This microwell geometry promotes the generation of cell aggregates (Ungrin *et al.*, 2008). The AggreWell plates were first treated with anti-adherence rinsing solutions (Stemcell Technologies, cat. no. 07010), centrifuged at 1300 g for 5 minutes then washed one time with basal medium. Then cell suspensions were added, pipetting up and down to more evenly distribute the single cells before the AggreWell plates were centrifuged at 100 g for 3 minutes. Then, the total volume in each well was increased to 2 mL for the 24 well pates and to 5 mL for the 6 well plates by adding complete DMEM. The AggreWell plates were placed in a humidified incubator at 37°C and 5% CO_2 for 72 h with half volume medium exchanges

every 24 h. At 72 h the aggregates were harvested from the AggreWell plate using wide bore pipet tips (TF-1005-WB-R-S, Axygen).

2.4 Shear Resistance Experiments

The energy dissipation rate (EDR) was calculated in order to estimate the applied shear forces on aggregates. For aggregate sturdiness the encapsulation process was simulated using spinner flasks and a magnetic stirrer (Section 4.1). During an encapsulation process the applied mean specific EDR value is almost 10^4 W/m^3, so to mimic these conditions aggregate suspensions were placed in spinner flasks. Then, a predetermined agitation rate was applied to assess aggregate durability at the calculated EDRs. This durability was determined by image analysis of the aggregates.

2.4.1 Image analysis of aggregates

First, aggregates were sampled in 50 µL aliquots and plated in a 384 well plate. These samples were photographed using a digital camera mounted on an inverted microscope (Motic, AE31 Elite Inverted Microscope), and the pictures analyzed using ImageJ software to determine the number of aggregates in each aliquot. For the image analysis the parameters were measured by using scale tool. For 2X objective, the image scale was determined as 0.992 pixels/µm. After all the samples were photographed at 2X, all images were opened with ImageJ and for each aggregate in the image a straight diameter with 0º angle was drawn using ImageJ drawing tool. Each diameter was then sized based on the determined scale

(0.992 pixels/μm). The total number of aggregates was calculated by extrapolating from the number estimated for each aliquot. By comparing the number of recovered aggregates to the initial number of aggregates, the aggregate recovery was determined.

Chapter 3: The Aggregation Model and Disaggregation

3.1 Aggregation and Aggregate Cultures

MIN6 cells are capable of glucose stimulated insulin secretion (Ishihara *et al.*, 1993; Skelin, Rupnik and Cencic, 2010). However, since islet cells are clusters consisting of mostly β cells plus α cells and other pancreatic islet cells, the sphere-shaped organization of islet cells impacts the function of insulin producing β islets. Thus, a similar aggregation of MIN6 cells is required to appropriately model and investigate transplantation and encapsulation of β cells. Therefore, the target was to generate MIN6 aggregates with a diameter of approximately 150 μm, a size similar to human islets.

3.1.1 Analysis of aggregation methods

3.1.1.1 Aggregation using shaking agitation

The effect of shear force generated from shaker agitation rate on aggregate formation from single cells was investigated as follows. Single cells were loaded into a 50 mL shake culture tubes and these shake tubes were set at 150, 200, 225, 250 and 300 rpm on an orbital shaker and at 225 rpm on a Kuhner shaking incubator. Using two different shaking platforms with two different throws (shaking amplitudes) enables a wide range of shear forces to be investigated, yet 225 rpm was the only available agitation rate in Kuhner shaker because it was specifically needed for the other ongoing experiments in the lab. Using the orbital shaker

either failed to form aggregates with settled dispersed cells at the bottom of the shake tubes or formed aggregates with diameters greater than 1 mm or smaller than 50 µm. Moreover, they also had nonspherical and non-uniform shapes (Appendix B.1). The aggregates generated at 225 rpm using the Kuhner shaker had more spherical and uniform shapes (Figure 3.1).

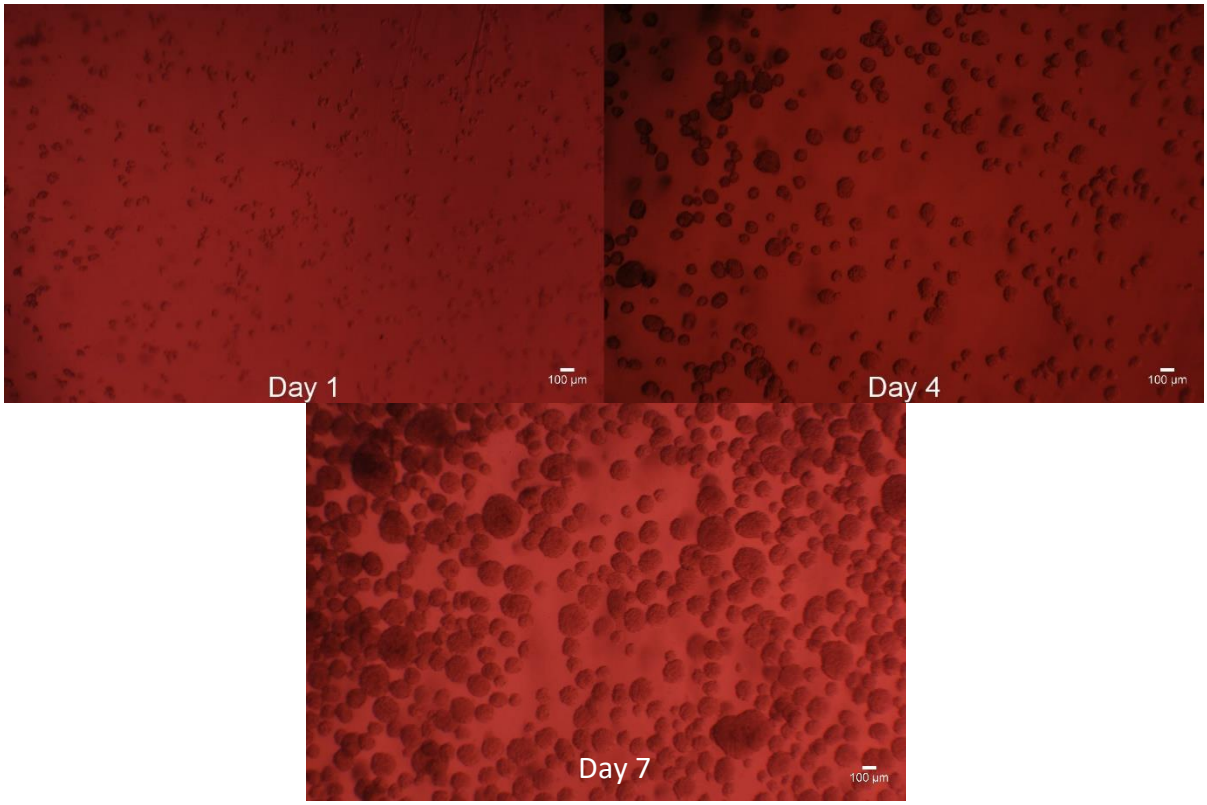

Figure 3.1 Aggregate generation over 7 days at 225 rpm in the Kuhner shaker.

Initially three different initial cell concentrations, $0.105x10^6$, $0.35x10^6$ and $1.05x10^6$ cells/mL, were loaded into the Kuhner shaker shake culture tubes. However, the lowest initial cell input did not effectively generate aggregates and most of the cells settled to the bottom of the shake culture tube (Figure 3.2).

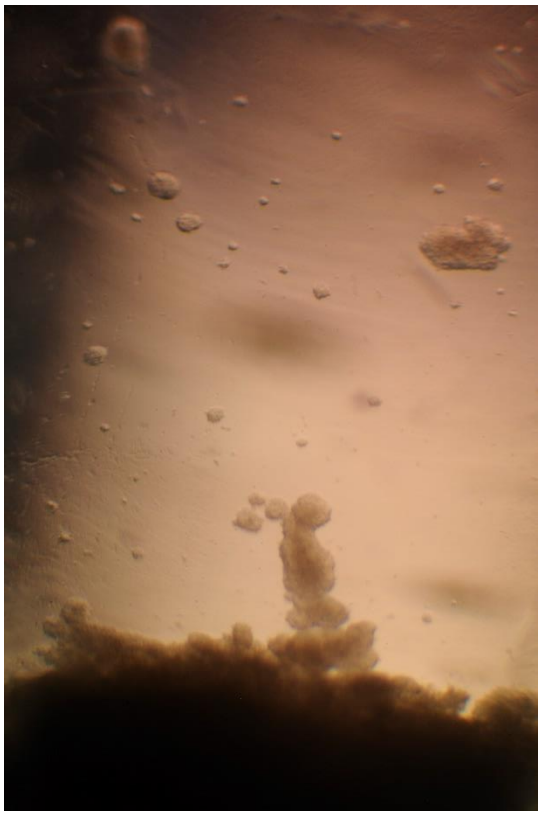

Figure 3.2 MIN6 cells with a $0.105x10^6$ cells/mL input cells on day 7.

Since the outcome of the lowest initial cell input was poor, further experiments were performed using the two higher initial inputs. The aggregation and size distribution results were compared and analyzed to select the initial cell input that would yield more uniform aggregate generation with the targeted diameter (Figure 3.3).

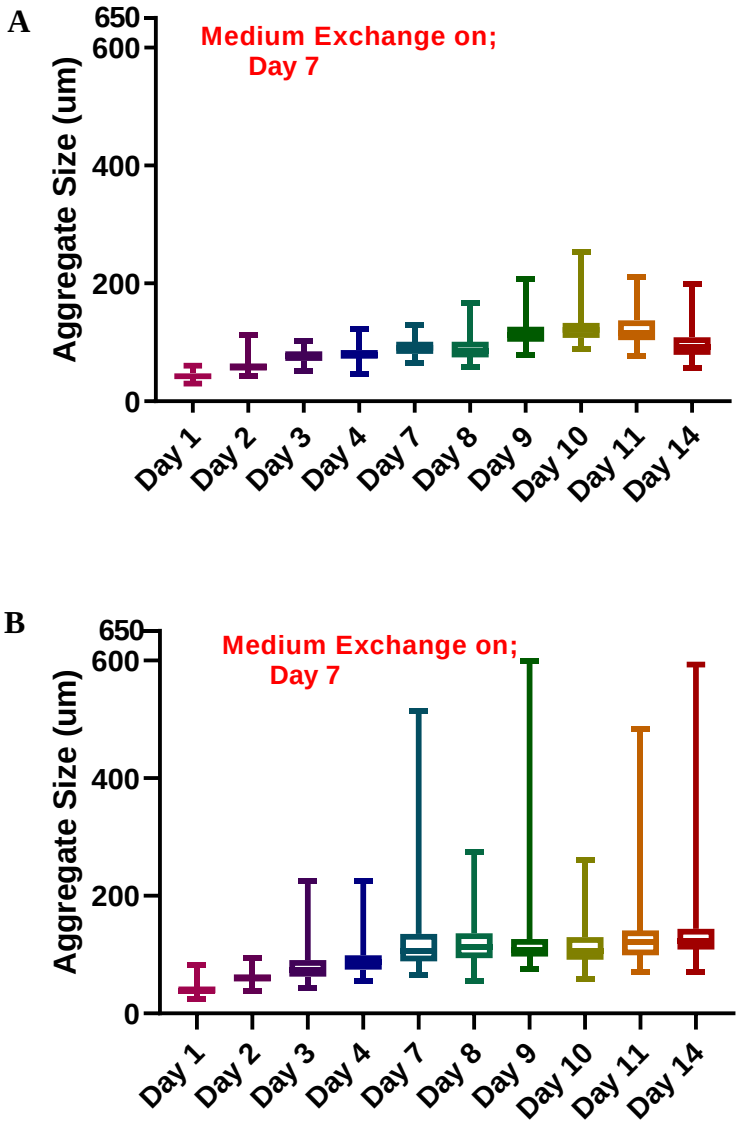

Figure 3.3 Size distribution in diameters of MIN6 cellular aggregates over 14 days.
(A) Diameters of MIN6 cellular aggregates with $0.35x10^6$ cells/mL initial single cell input. (B) Diameters of MIN6 cellular aggregates with $1.05x10^6$ cells/mL initial single cell input.

The cells were then cultured for two weeks with the medium changed once on day 7. Although there is a slight increase in aggregate diameters after the day 7 medium change, the aggregate diameters in both cases did not change significantly (Figure 3.3). The results are also listed in Table 3.1.

Table 3.1 Aggregate diameters of MIN6 cellular aggregates with $0.35x10^6$ cells/mL initial concentration and MIN6 cellular aggregates with $1.05x10^6$ cells/mL initial concentration over 14 days.

MIN6 Aggregates, Initial Single Cell Input: $0.35x10^6$ cells/mL[1]										
Days	**1**	**2**	**3**	**4**	**7**	**8**	**9**	**10**	**11**	**14**
Minimum	30	42	50	46	65	58	79	89	77	56
25% Percentile	38	52	69	73	81	75	101	105	101	79
Median	42	58	76	79	91	85	113	121	115	93
75% Percentile	48	64	85	87	101	101	126	133	137	109
Maximum	60	113	103	123	129	167	208	254	212	200
Mean	42	60	77	80	92	89	115	124	122	96
Range	30	71	52	77	65	109	129	165	135	143
IQR[2]	10	12	16	15	20	26	26	26	33	30
MIN6 Aggregates, Initial Single Cell Input: $1.05x10^6$ cells/mL[1]										
Days	**1**	**2**	**3**	**4**	**7**	**8**	**9**	**10**	**11**	**14**
Minimum	24	38	42	54	65	54	76	58	71	71
25% Percentile	36	54	62	75	89	94	97	91	98	109
Median	38	60	75	87	107	113	109	107	121	124
75% Percentile	44	67	91	99	135	136	126	130	141	144
Maximum	83	94	226	226	514	274	599	260	484	593
Mean	41	62	81	90	117	118	129	117	132	140
Range	58	55	183	171	450	220	523	202	413	522
IQR[2]	8	13	28	24	46	42	30	38	42	35

[1]The unit of all values is µm. [2]Inter Quantile Range; the difference between 25^{th} and 75^{th} percentiles.

On day 7, the average (mean) diameters of aggregates were 92 µm and 117 µm for low and high initial single cell concentrations respectively. Even though the average diameter of aggregates with the higher $1.05x10^6$cell/mL initial concentration was closer to the targeted diameter (150 µm), aggregates from the $0.35x10^6$cell/mL input concentration had a much narrower size distribution. Not only the range of values but also the inter quartile range (IQR)

of aggregate diameters from the higher initial cell concentration were higher. IQR is the difference between the 25^{th} percentile and the 75^{th} percentile of the diameter values of generated aggregates. Having a narrower size distribution was one of the desired outcomes. On day 7, the IQR value of the aggregates formed from the higher initial cell concentration was double that of the IQR value of the aggregates from the lower initial cell concentration. Moreover, in some samples the higher initial cell concentration resulted in aggregates with a diameter larger than 1 mm. This is much greater than the targeted diameter size and may result in core region necrosis due to insufficient mass transport of oxygen. Thus, the initial cell concentration for aggregate generation was selected to be $0.35x10^6$ cells/mL. All subsequent experiments were conducted using this initial concentration.

Aggregate suspensions were then cultured for 7 or 14 days to test the effects of medium exchange frequency on aggregate formation at 225 rpm and with an initial concentration of $0.35x10^6$ cells/mL. Either the medium was replaced every two days or on day 7. Figure 3.3 and Figure 3.4 show that after 7 days the average diameters of aggregates changed little. This confirms that aggregates can be generated from single cells without culturing more than 7 days. It was also observed that, after day 10 or 11, the aggregates start to lose their uniform spherical structure. In addition, these results also revealed that the higher rates of medium exchange had a positive effect on the aggregate sizes. Detailed results are listed in Table 3.2.

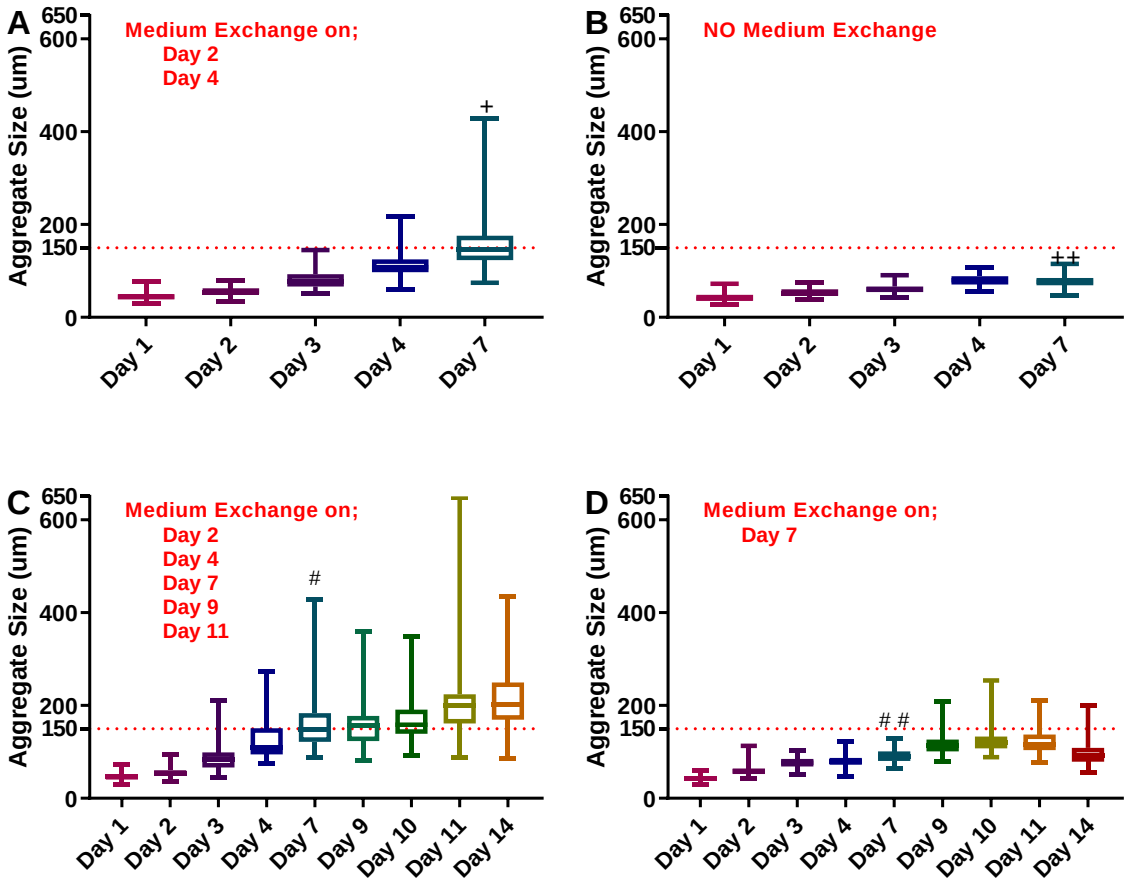

Figure 3.4 Effect of medium exchange and culture time on aggregate generation and size distribution (each n = 2).
(A) Medium exchange every 2 days and 7 days culture, $^{+}$SEM=4.2. (B) No medium exchange and 7 days culture, $^{++}$SEM=1.2. (C) Medium exchange every 2 days and 14 days culture, $^{\#}$SEM=5.3. (D) Medium exchange only once a week and 14 days culture, $^{\#\#}$SEM=1.3.

Table 3.2 Effect of feeding schedule and time on aggregate generation.

	MIN6 Aggregates[1] (Medium exchange every 2 days)					MIN6 Aggregates[1] (NO medium exchange)				
Days	**1**	**2**	**3**	**4**	**7**	**1**	**2**	**3**	**4**	**7**
25% Percentile	40	50	56	97	123	36	46	54	71	69
Median	44	54	76	107	147	40	52	60	80	77
75% Percentile	48	62	93	125	176	49	60	67	89	85
Mean	45	56	82	114	157	43	53	61	80	78
IQR	8	12	26	28	53	45	36	48	50	69

MIN6 Aggregates[1] (Medium exchange every 2 days)									
Days	**1**	**2**	**3**	**4**	**7**	**9**	**10**	**11**	**14**
25% Percentile	40	48	67	95	121	123	139	161	169
Median	46	54	83	110	149	156	158	201	202
75% Percentile	52	61	99	151	183	177	191	224	249
Mean	47	56	87	125	160	156	167	203	209
IQR	12	12	32	56	62	54	52	62	80

MIN6 Aggregates[1] (Medium exchange once a week)									
Days	**1**	**2**	**3**	**4**	**7**	**9**	**10**	**11**	**14**
25% Percentile	38	52	69	73	81	101	105	101	79
Median	42	58	77	79	91	113	121	115	93
75% Percentile	48	64	85	87	101	126	133	137	109
Mean	42	60	77	80	92	115	124	122	96
IQR	10	12	16	15	20	26	26	33	30

[1]The unit of all values is μm.

From the table it can be seen that aggregates fed every 2 days reached the targeted 150 μm diameter with an average diameter of 160 μm on day 7. Aggregates fed once a week only reached an average diameter of 92 μm on day 7 and when they were cultured beyond 7 days, these aggregates failed to achieve the targeted diameter. Furthermore, it was also observed

that feeding the cultures every two days enabled aggregates to maintain their uniform spherical shapes compared to aggregates fed only once a week that lost their uniform structures, and even disassembled 3-4 days after medium change. Thus, the selected aggregate culture conditions were in 50 mL tubes at 225 rpm in a Kuhner shaker, with a $0.35x10^6$ cells/mL initial cell concentration, feeding every 2 days up to 7 days.

3.1.1.2 Effect of serum in medium on aggregate generation

Fetal bovine serum (FBS) is a supplement for cell culture media. FBS supplies a mixture of proteins and other growth factors to the medium (Bieback *et al.*, 2009). Many different studies (Sakai *et al.*, 2004; Cabrera *et al.*, 2006; Huang, Ramachandran and Stehno-Bittel, 2013; Yang *et al.*, 2013; Hilderink *et al.*, 2015; Vlahos, Cober and Sefton, 2017) and a previous study conducted in the Piret Lab (Hoesli *et al.*, 2011), all use DMEM supplemented with 10% (v/v) FBS for MIN6 cell culture. The effect, if any, of FBS on aggregate generation was analyzed by increasing the fraction of FBS added. For this purpose, in 7 day batch cultures, one aggregate suspension was cultured in DMEM with 10% FBS (control) and two other aggregate suspensions were cultured in DMEM with 20% FBS. The initial cell concentration was $0.35x10^6$ cell/mL and tubes placed in the Kuhner shaker at 225 rpm.

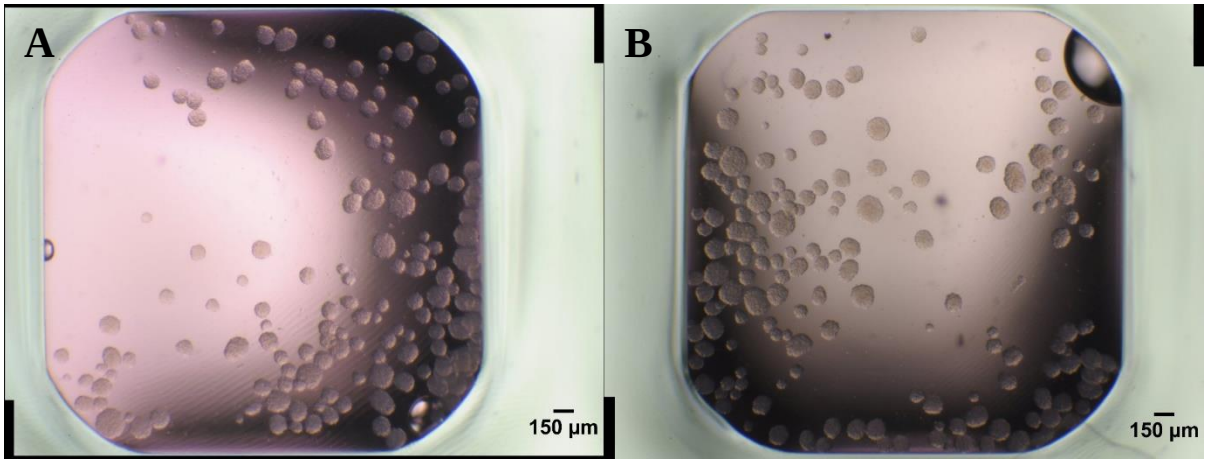

Figure 3.5 MIN6 cellular aggregates after harvested on day 7.
(A) Aggregates cultured in complete DMEM with 10% FBS. (B) Aggregates cultured in complete DMEM with 20% FBS.

On day 7 when the cells were harvested and analyzed, there was little difference between the aggregate shape and size distribution for both conditions (Figure 3.5 and Figure 3.6A). The average diameters are 126 µm and 122 µm for the 10% FBS and 20% FBS conditions, respectively. The aggregates from these two populations were very similar in size with the mean diameter value of the aggregates cultured in DMEM with 20% FBS slightly smaller than the control ones. Similarly, the 75^{th} percentile of the aggregate size on both conditions were distributed around similar values; 145 µm for the control and 141 µm for the protocol.

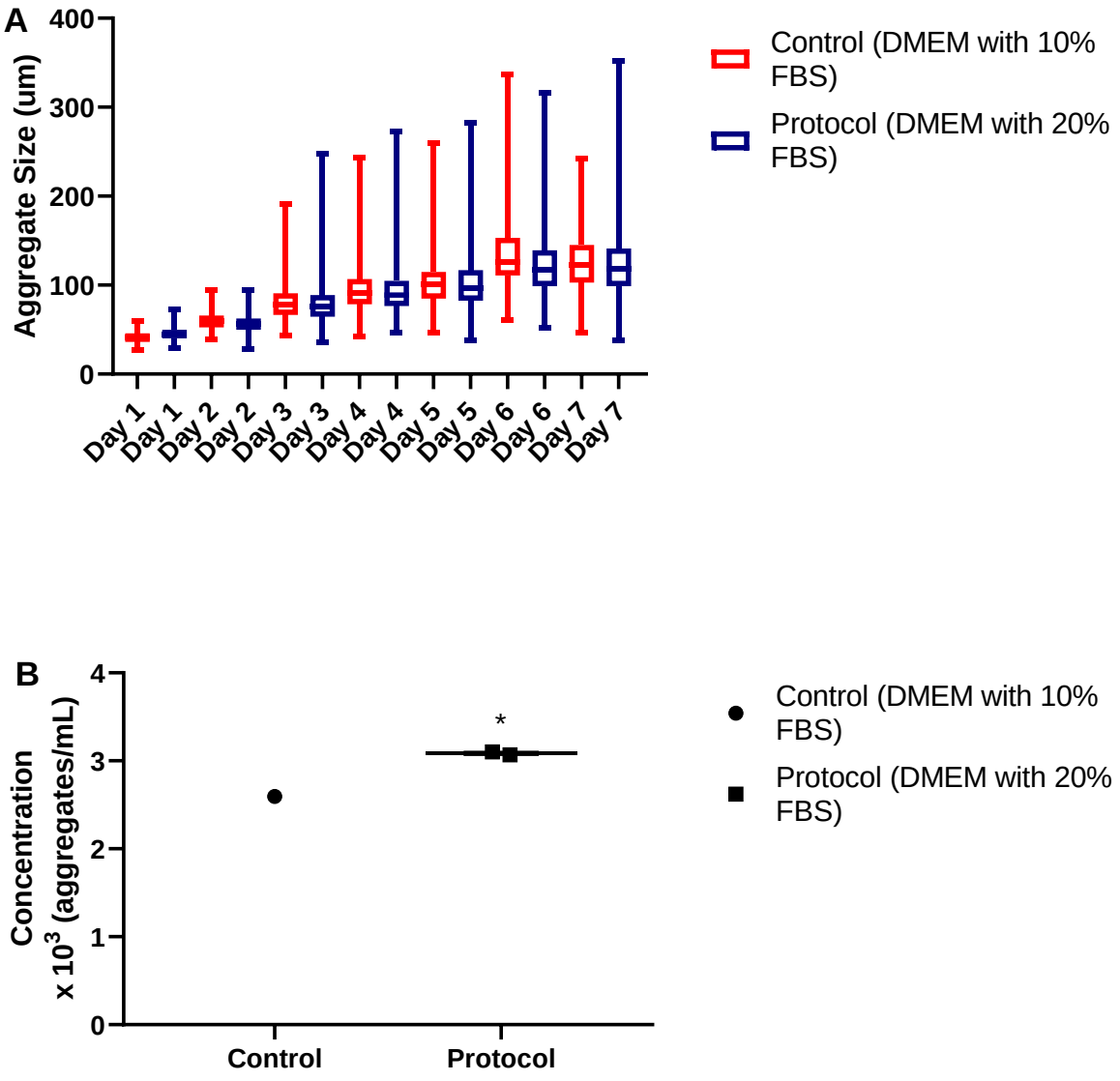

Figure 3.6 Effect of FBS ration in medium on aggregate generation.
(A) The size distribution of aggregate diameters over 7 days. Red box & whiskers represents the control and the blue ones represent the duplicated 20% serum condition (B) Aggregate concentrations on day 7 when the aggregates are harvested (*n=2, SEM=0.01)

On day 7 the aggregate concentrations were calculated and (Figure 3.6B) again no significant difference was observed. In both conditions the aggregate concentrations were $2.6x10^3$, and $3.1x10^3$ & $3.1x10^3$ aggregates/mL for 10% FBS and 20% FBS (duplicated) conditions, respectively. Since there is no significant impact on aggregates size or numbers obtained

from increasing the FBS concentration in DMEM. The subsequent experiments continued to be performed with DMEM supplemented with 10% (v/v) FBS.

3.1.1.3 Aggregation without shaking

The aggregation generation method using shake culture tubes in the Kuhner shaker generated aggregates with an average diameter close to the 150 µm target. However, the wide size distribution range and not very favourable sturdiness of the resulting aggregates (discussed in Chapter 4) motivated exploring a new approach to generate aggregates.

A static aggregation method was investigated as an alternate procedure to form aggregates. Commercially available AggreWell plates (AggreWell^{TM} 400, Stemcell Technologies, cat. no. 34411&34421) were tested for this purpose. Although AggreWell plates were initially designed to generate embryonic bodies for stem cells and spheroids for particular cell lines (Ungrin *et al.*, 2008), they can be used for many kinds of cells. They are 6 or 24 well plates, with each well consisting of microwells that are either 400 µm or 800 µm in size. The square-based inverted pyramid shape of these microwells permits formation of aggregates with the aid of centrifugal force. In this study, 6 and 24 well 400 µm AggreWell plates were used for aggregate generation. The 6 well AggreWell plates have 7000 microwells in each well, whereas 24 well plates have 1200 microwell in each well. For both 6 well or 24 well AggreWell plates, the aggregate generation process was described in Section 2.3. The AggreWell plates comes with a protocol for aggregation and includes the rinsing solution. The aggregation method defined in section 2.3 is based on this protocol with some

customization for MIN6 aggregation. The rinsing solution enables the aggregates to be easily dislodged from the plate. For a 24 well plate the initial concentration was $0.5x10^6$ cell/mL which combined 1 mL of single cell suspension with 1 mL of fresh complete DMEM. For a 6 well plate the initial concentration was $1.0x10^6$ cell/mL using 3 mL of single cell suspension plus 2 mL of fresh complete DMEM. After the single cells were evenly distributed in microwells via centrifugation at 1300 g, they were cultured in an incubator for 3 days and the resulting aggregates harvested (Figure 3.7A). They had a spherical structure after recovery from the plate (Figure 3.7B). In general, aggregates generated in AggreWell plates had a more spherical structure than aggregates generated in shake tubes. Also, the culturing time for aggregate generation is less than the one week required for aggregates generated in shake tubes. Size analysis results showed that aggregates generated with AggreWell plates had a much narrower size distribution compared to aggregates generated in shake tubes (Figure 3.8).

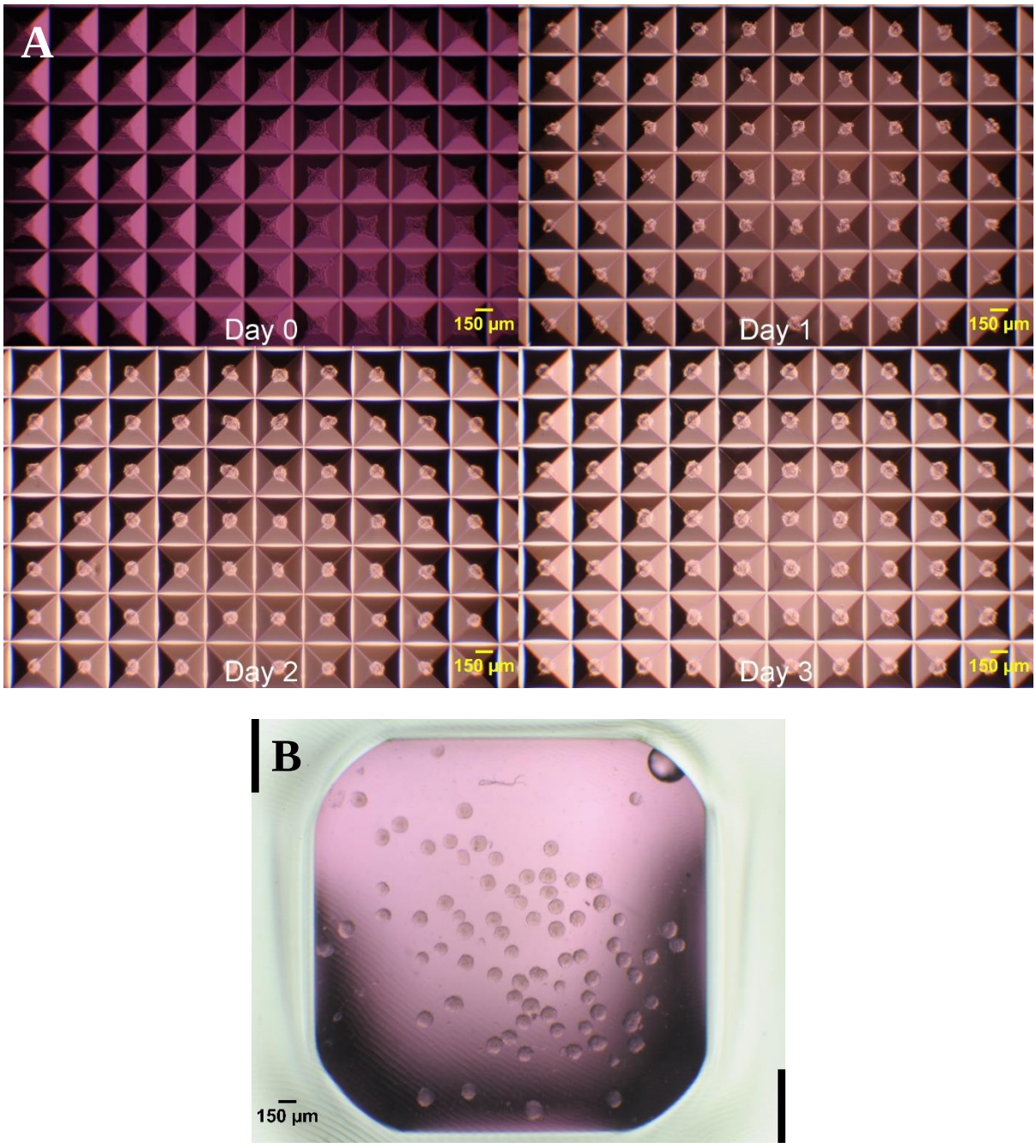

Figure 3.7 (A) Formation of aggregates over 3 days in an AggreWell plate. (B) Aggregates after the harvest on day 3.
Aggregation of cells in the center of each microwell can be distinguished.

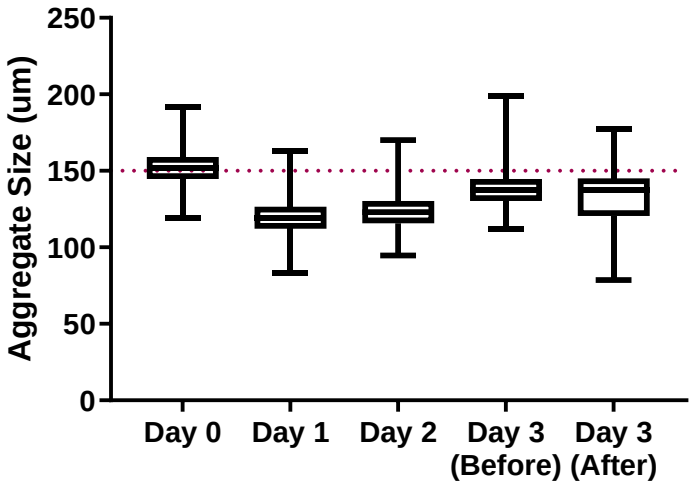

Figure 3.8 Size distribution of aggregates over 3 days in AggreWell plate.
Before and after results on day 3 represent the size distribution before and after aggregates were harvested.

The average diameter in the AggreWell plates was ~150 µm on day 0 (Figure 3.8). Apparently, as aggregates developed a more spherical shape, this decreased the size distribution on day 1. Nonetheless, over 3 days the mean diameter increased towards the targeted 150 µm diameter and the harvested aggregate size distribution was narrower than from the shake tubes, with the 90^{th} percentile at 152 µm and the 10^{th} percentile at 123 µm. AggreWell plate aggregation had many advantages compared to aggregation in shake tubes, i.e. shorter culture time, more uniform aggregate shape and a narrower size distribution. AggreWell plates were used for aggregate generation for the rest of the experiments except in conditions used to compare the sturdiness of the aggregates generated by both methods.

3.2 Disaggregation of Aggregates Generated in AggreWell Plates

A controllable disaggregation method was developed for the analysis of the cell content of aggregates after exposure to external shear forces. Thus, a controllable protocol was needed for disaggregation into individual cells. Accordingly, an enzymatic disassociation agent (TrypLE, Gibco cat. no. 12605010) and agitation forces (Kuhner shaker) were used to gently disperse aggregates into single cells. Firstly, static disaggregation without any stirring or agitation forces using only disassociation agent was studied. Then, several combinations of TrypLE volumes and shaking/incubation times were investigated to optimize the disaggregation method. The aim of trying different volumes of TrypLE and different shaking times was to avoid excessive digestion and shear force while maximizing disaggregation performance. All disaggregation experiments were conducted immediately after aggregates were harvested from AggreWell plates.

3.2.1 Disaggregation without agitation

For disaggregation without agitation, 3 x 2 mL of harvested aggregate suspension (845 aggregates/mL) were transferred into 3 x 15 mL shake tubes to have 3 analytical replicates. After they were centrifuged at 100 g for 2 minutes, the supernatant in each shake tube was removed and replaced with 1 mL TrypLE. Then all shake tubes were placed inside a 37℃ incubator without shaking or agitation. Samples were removed every 10 minutes for 30 minutes. For imaging, 50 µL samples were drawn from each tube and all these aliquots were plated in 384 well plate for size distribution analysis (Figure 3.9A).

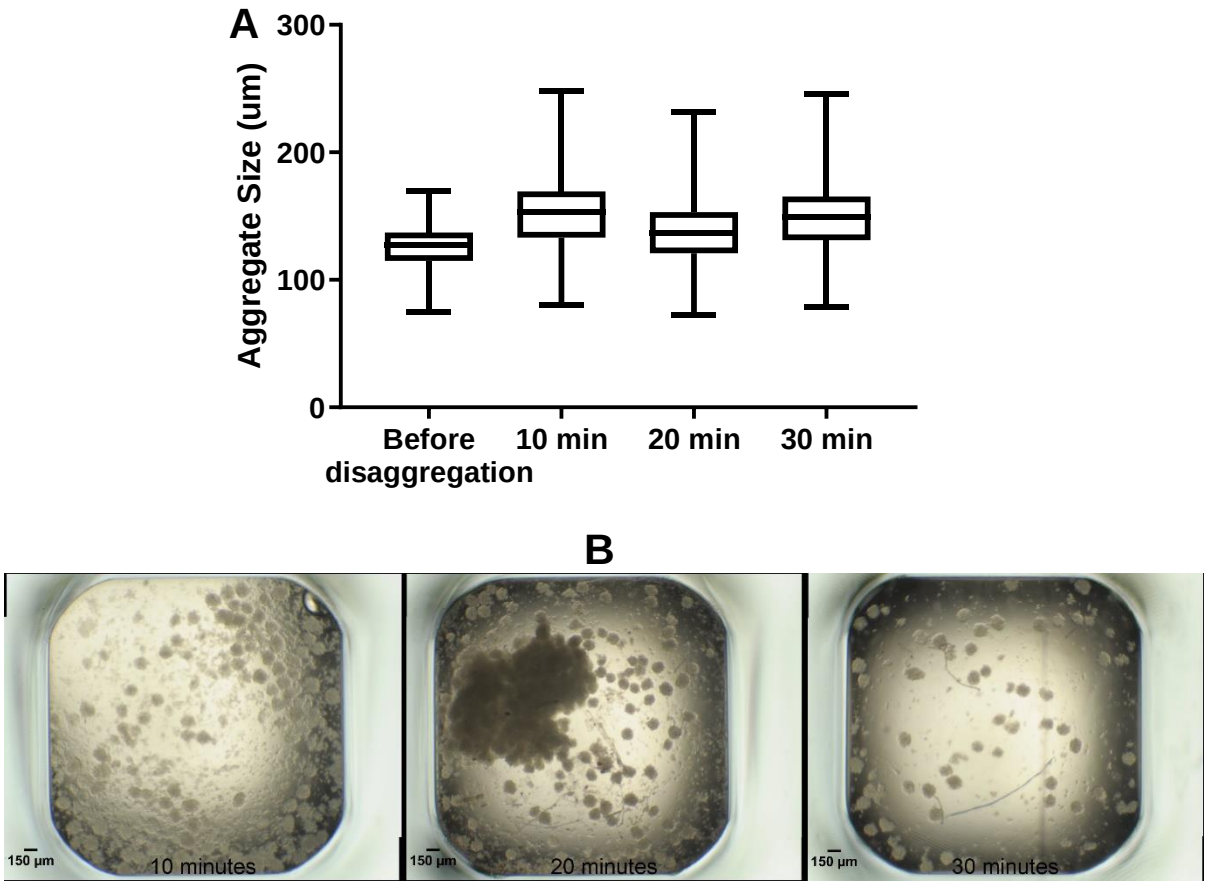

Figure 3.9 (A) Size distribution of aggregates during disaggregation treatment. (B) Effect of static disaggregation on aggregates over 30 minutes.

Images (Figure 3.9B) show that leaving aggregates in TrypLE solution without agitation is not enough to disaggregate them into single cells (Figure 3.9A). It was observed in some cases that some of the aggregates combined to form larger aggregates even in the presence of the TrypLE.

3.2.2 Disaggregation using agitation

The incubation time of aggregates in TrypLE combined with shaking at 225 rpm was then investigated. Accordingly, three different time points, 20, 40 and 60 minutes were selected and for each time point three analytical replicates were analyzed. After size analysis, the aggregate suspensions were transferred into 50 mL shake tubes and their supernatant was removed after centrifugation. Next, 5 mL of TrypLE was added to each tube and all nine samples were placed in the Kuhner shaker at 225 rpm and 37C. Three tubes were taken out at each time point and counted using a Cedex Cell Analyzer. Figure 3.10 shows the disaggregation results in terms of aggregate diameter. At all three time points the average diameters were reduced to the 10 ~ 11 μm diameter of single cells. This result suggested that even shorter incubation times with TrypLE may be sufficient. Before trying shorter incubation times, decreasing the volume of TrypLE from 5 to 1 mL was analyzed for samples exposed to shaking for 60 minutes. The resulting disaggregation was found to match the 5 mL results (Figure 3.10).

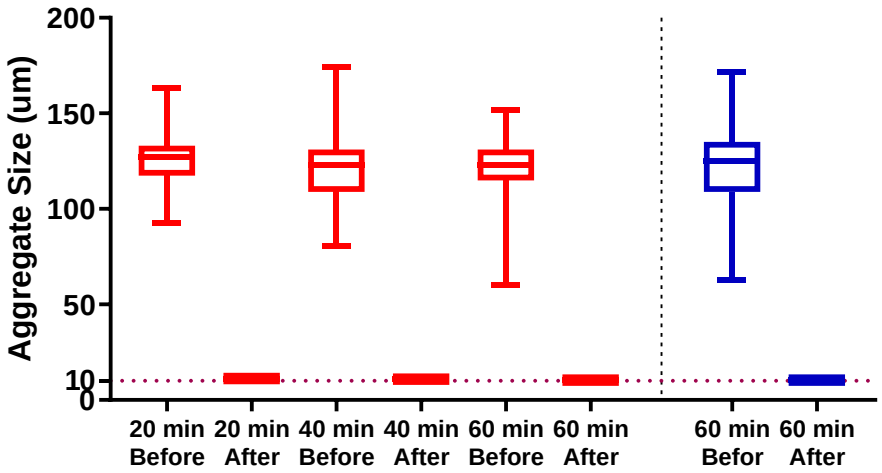

Figure 3.10 Size distribution of aggregate diameters before and after disaggregation (n=3).
The red boxes demonstrate the time course experiments where the aggregates from the same batch were treated with 5 mL TrypLE solution at 225 rpm for different times. The blue box demonstrates the results of disaggregation with less volume of TrypLE solution (1 vs. 5 mL) at 225 rpm for 60 minutes.

Subsequent disaggregation experiments were performed using 1 mL of TrypLE at incubation times of 10, 20 and 30 minutes and 225 rpm shaking. Three different biological replicates with two different analytical replicates for each point were analyzed for size distribution to confirm disaggregation (Figure 3.11). Again, the shorter time periods yielded single cell diameters (~10 µm) within the first 10 minutes of TrypLE exposure, with shaking.

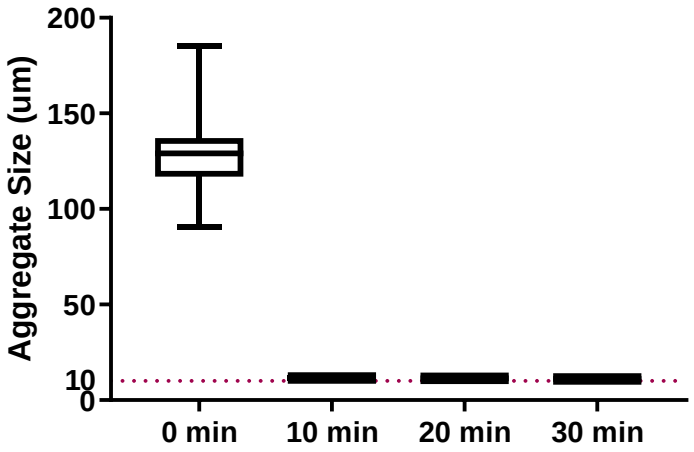

Figure 3.11 Size distribution in aggregate diameters before and after disaggregation over 30 minutes (n=3).

Although the TrypLE method was effective for disaggregation, a concern was that the TrypLE solution and shear may either cause some of the cells to become nonviable or be further damaged so that they are not even counted. Thus, $1.0x10^6$ single cells, corresponding to the number of cells required to generate 2400 aggregates were treated as single cells with 1 mL of TrypLE at 225 rpm for 30 minutes. The results were analyzed as a control condition, and compared to the disaggregation results of aggregates.

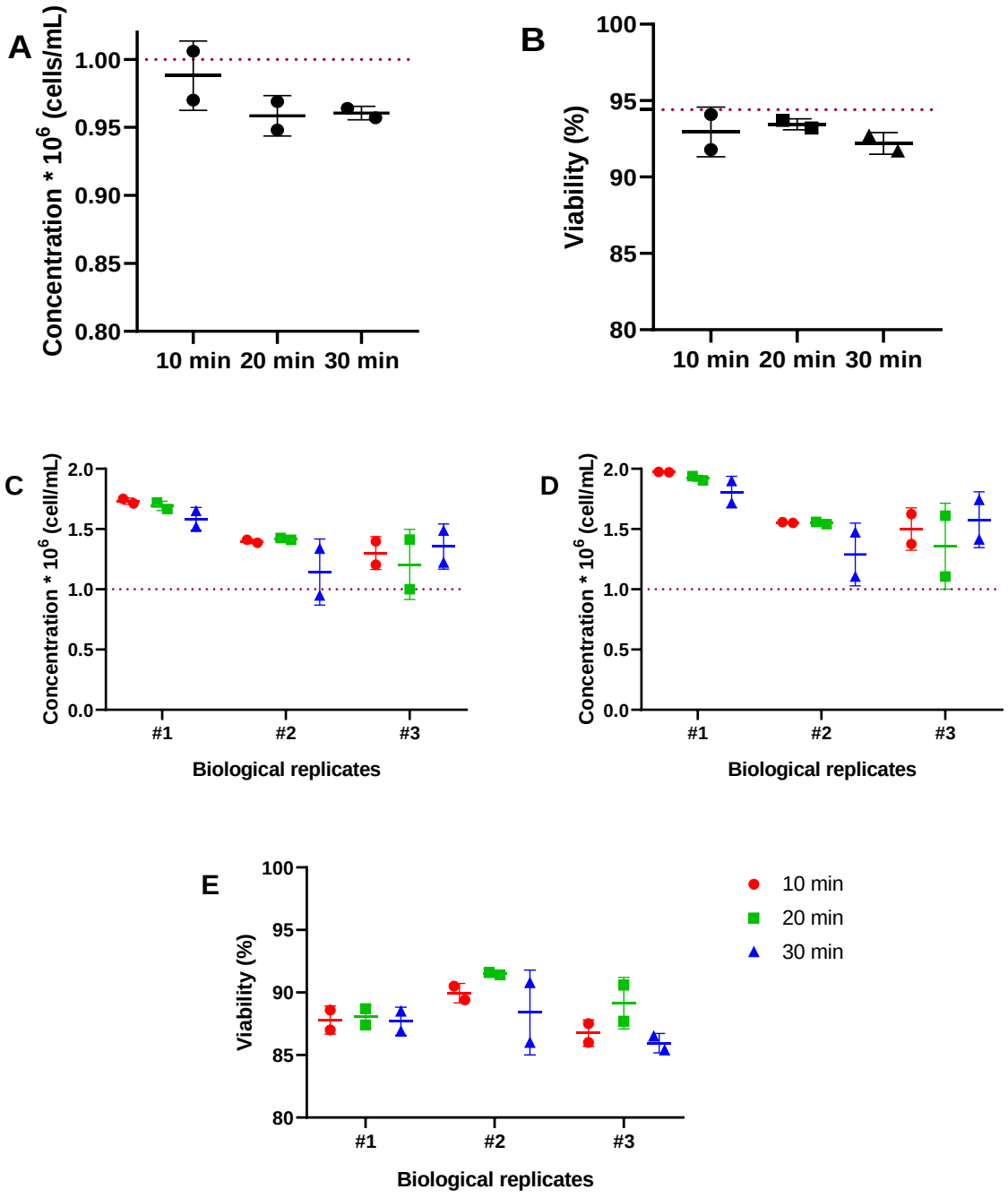

Figure 3.12 Cell recovery results from single cells and disaggregated cells treated with TrypLE. Single cell control: The change of total cell concentration (A) and the cellular viability (B) of single cells. Dotted lines are the initial concentrations and initial cellular viability (94.4%) before treatment (n=2). Disaggregated cells: Viable cell concentration (C), total cell concentration (D) and cellular viability (E) of disaggregated cells during 30 minutes disaggregation treatment for each replicate (#1,#2, and #3). Dotted lines are the initial cell input to the AggreWell plates on day 0.

The cell enumeration results of TrypLE treated single cells (control) remained constant even after 30 minutes of TrypLE exposure (Figure 3.12A). Additionally, the cellular viability of single cells (control) did not significantly change through the entire treatment (Figure 3.12B). These results confirmed that the TrypLE exposure itself should not impact the cell enumeration results of disaggregated cells. Hence, the Figure 3.12C and D increase in the viable cell and total cell numbers compared to the cell input on day 0 ($1.0x10^6$ cells) is due to cell proliferation over 3 days. It can also be seen from the same graphs that the viable and total cell numbers do not change significantly with increasing exposure time to the TrypLE. Likewise, the stable cellular viability over 30 minutes (Figure 3.12E) revealed no negative effect on the cells. Thus, the conditions for disaggregation were selected to be in 1 mL TrypLE solution at 225 rpm in Kuhner shaker for 10 minutes.

3.2.3 Cellular growth and viability of aggregates generated in AggreWell plates

Because the aggregation in the AggreWell plates was performed over three days, the cellular viability of aggregates during this time period was investigated. For this purpose, on each day ~4800 aggregates ($2.0x10^6$ single cell day 0 initial cell input) were disaggregated using 1 mL of TrypLE at 225 rpm in Kuhner shaker for 10 minutes, followed by cell enumeration by Cedex. These results were plotted on Figure 3.13.

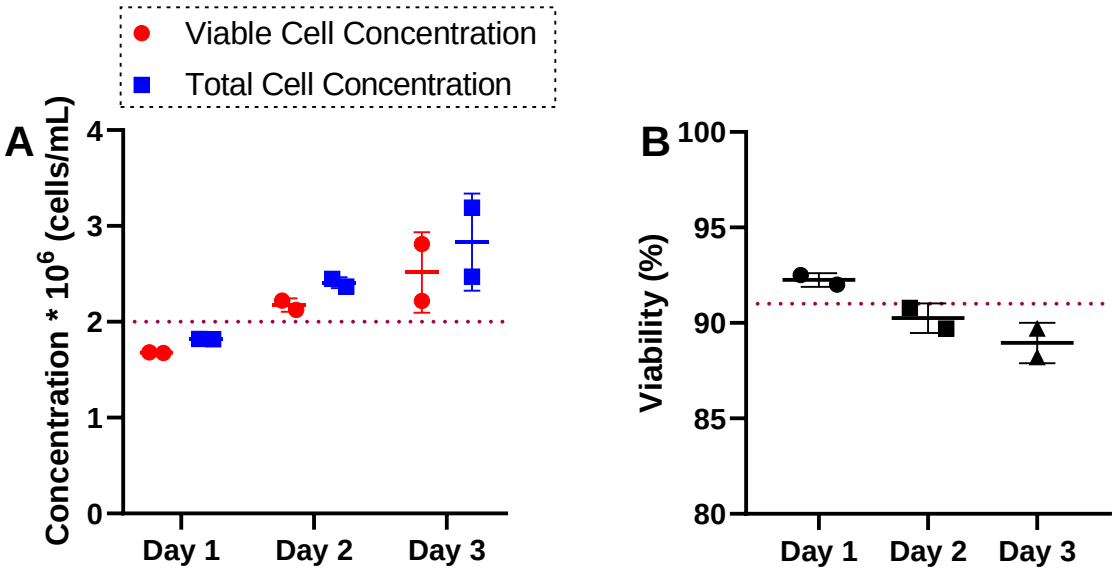

Figure 3.13 Cell growth and the viability of aggregates over 3 days.
(A) The change in the viable and total cell amount versus the initial cell input – Dotted line is the initial cell input (n=2). (B) The cellular viability of aggregates – Dotted line is the cellular viability (91%) of initial single cell suspensions loaded into AggreWell plate on day 0 (n=2).

The day 2 and day 3 apparent cell growth, also seen in Figure 3.13A, was similar to MIN6 cell growth in a T-flask (Appendix A.1). There were 9% and 26% increases in cell numbers compared to the initial cell input on days 2 and 3, respectively. The viability of aggregates may have declined over the 3 days (Figure 3.13B), but remained similar to the viability of the day 0 cell input.

Chapter 4: Shear Resistance of Aggregates and Analysis of Microcapsule Alginate Concentration

4.1 Analysis of Shear Stress Acting on Aggregates

Encapsulation is the process whereby cells are surrounded with a semipermeable alginate barrier. This was performed in this work using an emulsification and internal gelation method previously introduced by Hoesli (2010; Hoesli *et al.*, 2011). As explained in the Section 2.2, this encapsulation of cells is achieved using spinner flask agitation to emulsify the alginate solution in mineral oil. The alginate capsule formation was completed by internal gelation. During this process aggregated cells were exposed to shear forces generated by the agitation rate and influenced by the vessel geometry and the physical properties of the reagents. It was therefore necessary to investigate the sturdiness of aggregated MIN6 cells to ensure a successful encapsulation outcome. The mean energy dissipation rate (EDR) was used to quantify the shear force exposures. As discussed in Section 1.4.2, EDR is a scalar value that takes into account hydrodynamic factors in a bioprocess. Vessel dimensions (Table 4.1) and the physical properties of mineral oil (Table 4.2) were used to quantify the impeller power number and the mean EDR in the emulsification and internal gelation process. The final total volume in the spinner flask was 100 mL using either the paddle or the grid impeller (Appendix B.2). In the actual process, 30-40 mL of the final volume was mineral oil. However, since there is no impeller power number correlations for partially filled vessels, the spinner flask was assumed to be filled with 100 mL of mineral oil.

Table 4.1 Dimensions of spinner flasks and paddle impeller.

Dimension	Symbol	Value	Units
Vessel diameter	D	0.058	m
Liquid height	H	0.04	m
Impeller diameter	d	0.05	m
Impeller height	B	0.025	m
Impeller blades	n_b	2	
Impeller blade angle	θ	1.57	rad

Table 4.2 Physical properties of mineral oil.

Dimension	Symbol	Value	Units
Density	ρ	830	$kg \cdot m^{-3}$
Viscosity	μ	0.034	$kg \cdot m^{-1} \cdot s^{-1}$
Kinematic viscosity	ϑ	$4.145 \cdot 10^{-5}$	$m^2 \cdot s^{-1}$

After defining the geometric and physical parameters and using estimation of the paddle impeller power number (Appendix A.2), the mean EDR, $\bar{\varepsilon}$, for the encapsulation process can be calculated by dividing the power consumption of the impeller by volume of the liquid in the spinner flask:

$$\bar{\varepsilon} = \frac{N_P \rho N^3 d^5}{V} \qquad \textbf{Equation 4.1}$$

where N_P is the impeller power number, N is the agitation rate (s^{-1}), d is the impeller diameter, ρ is the fluid density, and V is the fluid volume.

The highest agitation rate attained during the encapsulation process was 1000 rpm (16.7 s^{-1}) and the corresponding mean EDR in the spinner flask was estimated based on the dimensions and the physical properties of mineral oil given in Table 4.1 & 4.2 and the impeller power number (Appendix A.2):

$$\bar{\varepsilon} = \frac{(8.9 \times 10^{-1})(830\ kg/m^{-3})(16.7\ s^{-1})^3(0.05\ m)^5}{0.0001\ m^3} = 1.07 \times 10^4\ W/m^3$$

For the shear resistance experiments mineral oil was replaced by basal DMEM to maintain the cells viable and in suspension. Thus, the agitation rates required were calculated from the mean EDR values based on the physical properties of water (Table 4.3), assumed to be the same as the physical properties of basal DMEM (i.e. DMEM without FBS). To avoid splashing of the much less viscous DMEM, the volume agitated was reduced from 100 mL to 30 mL. When the spinner flask was filled 30 mL of DMEM, the impeller was not completely submerged in the liquid. However, the suggested impeller power number correlations (Appendix A.2) take into account only completely submerged impellers. Therefore, for the estimation of impeller power number and mean EDR values, the paddle impeller was assumed to be completely submerged in the DMEM. Table 4.4 lists the other mean EDR values and the calculated corresponding agitation rates. The impeller power consumption assumptions could not be applied to the grid impeller because of its far more complex wired

lattice structure (Appendix B.2). Instead, the calculated agitation rates for the paddle impeller were matched in grid impeller experiments, and the results of those experiments are shown in Appendix A.3 since the shear exposure was less well defined. Nonetheless, those results were similar to the results presented here.

Table 4.3 Physical properties of water.

Dimension	Symbol	Value	Units
Density	ρ	1000	$kg \cdot m^{-3}$
Viscosity	μ	$8.90 \cdot 10^{-4}$	$kg \cdot m^{-1} \cdot s^{-1}$
Kinematic viscosity	ϑ	$1.787 \cdot 10^{-6}$	$m^2 \cdot s^{-1}$

Table 4.4 EDR values and corresponding agitation rates.

EDR (W/m^3)	Agitation rate (rpm)[1]
10^2	175 (~180)
10^3	416 (~420)
2.5×10^3	580 (~580)
10^4	975 (~980)

[1]The agitation rate displayed on the magnetic stirrer can only be adjusted in 10 rpm increments.

4.1.1 Effects of shear forces on aggregates generated in shake tubes

Aggregates generated in shake tubes were exposed to the agitation rates from Table 4.4 for 30 minutes, and then sampled at discrete time points to be analyzed for aggregate recovery.

A total shear-exposed processing time of 30 minutes was selected because the emulsification time varies from 1 minutes to 15 minutes, followed by a 3 minute acidification time, a 1 minute neutralization and a 10 minute curing step. Samples taken every 10 minutes were analyzed for the aggregate number, and by extrapolation, the total number of aggregates were estimated at that particular time point. All of the aggregate numbers from each time point were compared to the (100%) initial aggregate input number to calculate the recovery (Figure 4.1).

As seen in Figure 4.1A, the recovery for the EDR of 10^2 W/m^3 was high. However, this EDR is low compared to typical EDR values encountered during the encapsulation process. Recovery decreased with increasing EDR. At an EDR of 10^4 W/m^3 (the highest mean EDR of the encapsulation process) the recovery decreased to 0% within the first 10 minutes. Therefore, these results showed that aggregates generated in shake tubes do not have sufficient shear resistance.

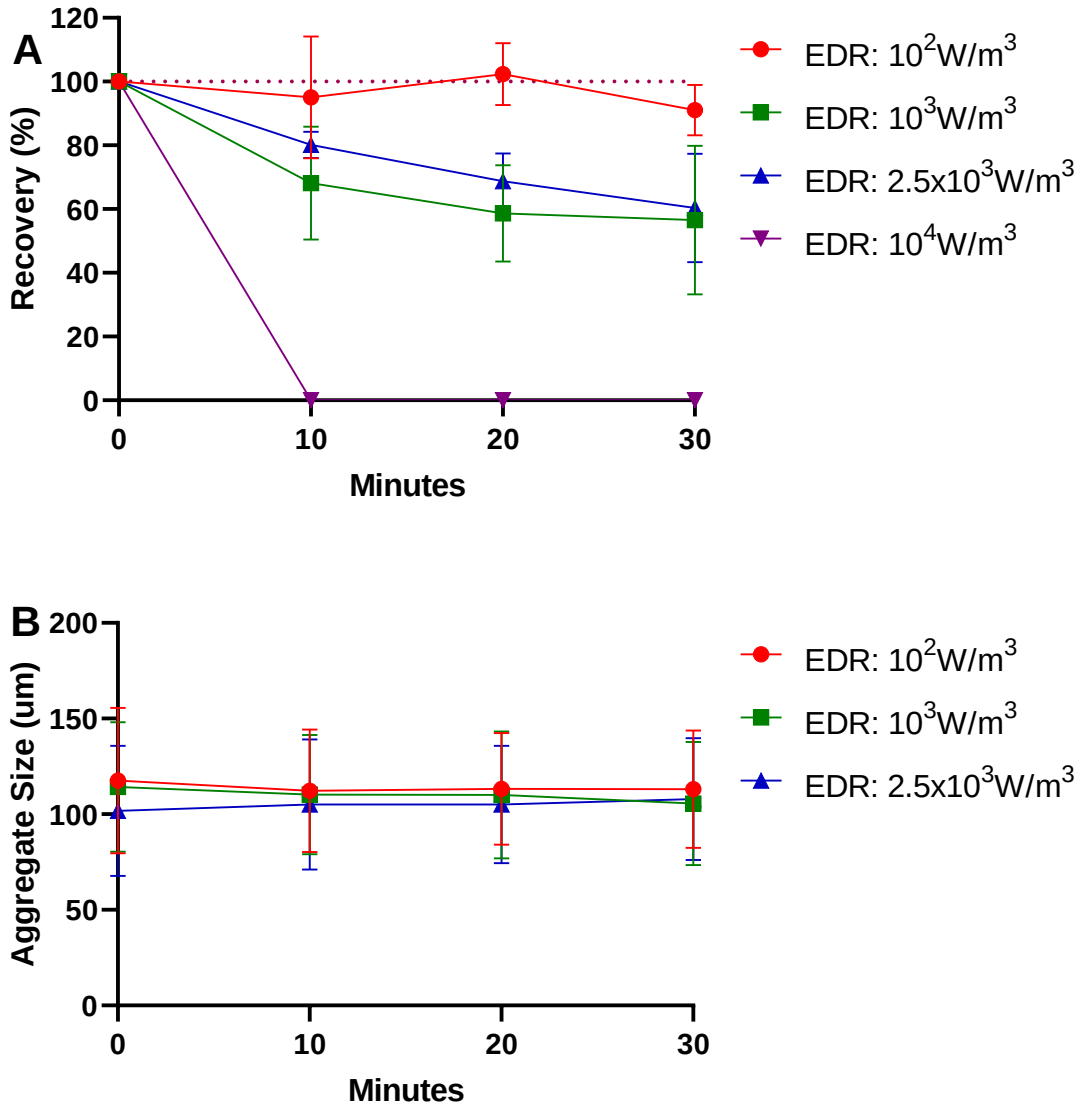

Figure 4.1 (A) Shake tube aggregates recovery after exposure to shear stress using a paddle impeller spinner flask (n=2). (B) Size distribution of recovered shake tube aggregates after exposure to shear stress using a paddle impeller spinner flask (n=2).
0 minutes size distribution results are before exposure to shear.

4.1.2 Effects of shear forces on aggregates generated in AggreWell plates

Aggregates generated in AggreWell plates (without shaking) were then exposed to the agitation rates from Table 4.4 to determine their recoveries (Figure 4.2A).

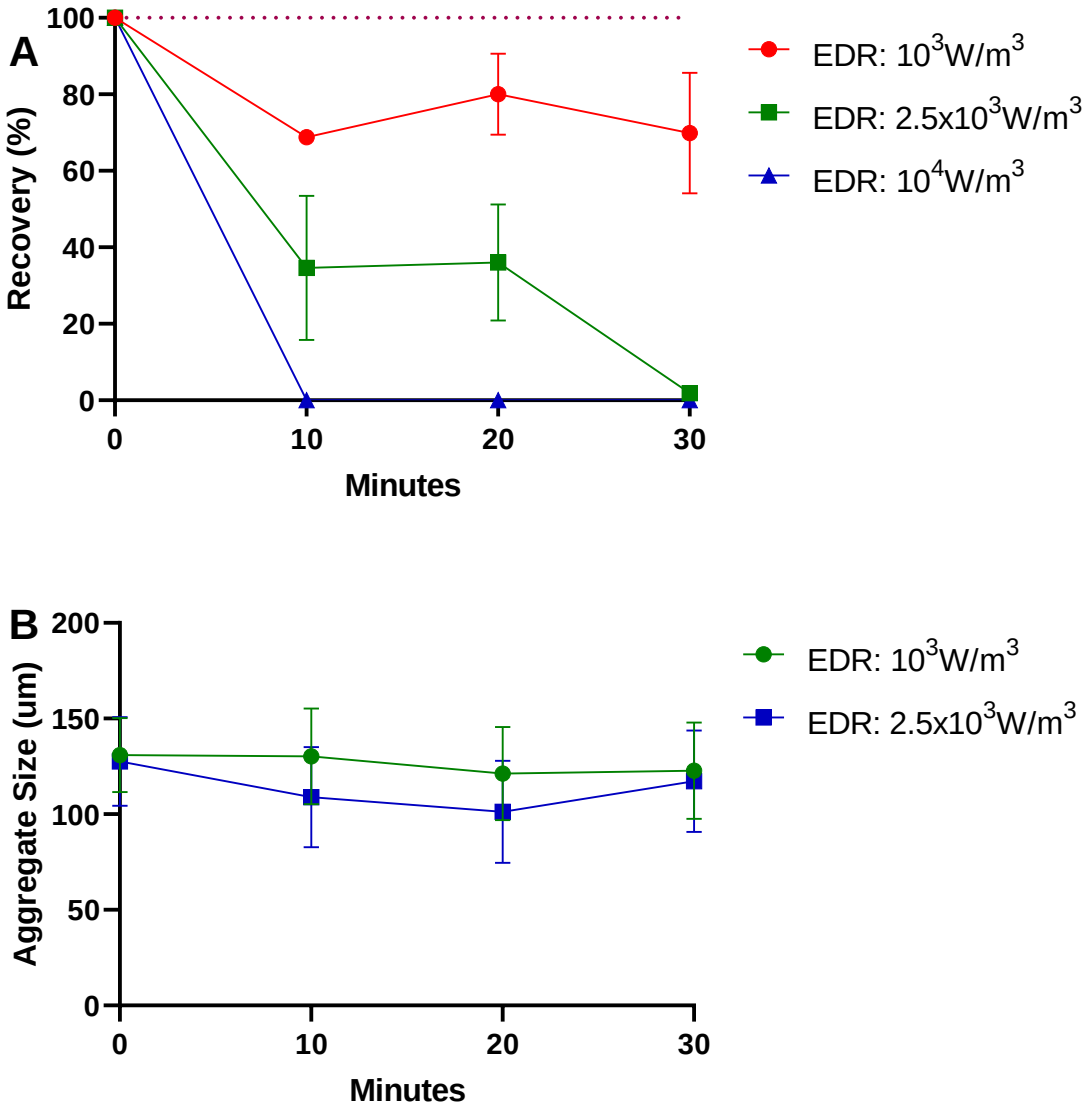

Figure 4.2 AggreWell plate aggregates recovery after exposure to shear stress using a paddle impeller spinner flask (n=2). (B) Size distribution of recovered AggreWell plate aggregates after exposure to shear stress using a paddle impeller spinner flask (n=2).
0 minutes size distribution results are before exposure to shear.

As found with aggregates generated in shake culture tubes, the aggregate recovery declined with increasing EDR values. At an EDR of 10^3 W/m^3 the recoveries were high, ~70% at 30 minutes. At an EDR of $2.5x10^3$ W/m^3 the recovery decreased to 0% at 30 minutes. At an EDR of 10^4 W/m^3 the recovery decreased to 0% within 10 minutes. Interestingly, the

aggregates formed in the shaking tubes were more shear resistant than those from the AggreWell plates. For example, at 30 minutes and an EDR of $2.5x10^3$ W/m^3 over 50% of the aggregates from the shake tubes were recovered (Figure 4.1A) whereas none of the AggreWell aggregates were recovered (Figure 4.2A). Moreover, the mean aggregate diameters were measured for aggregates before and after exposure to the shear. It was observed that the mean diameters of the recovered aggregates after shear exposure remained the same as the mean diameters of the aggregates before the shear exposure for both shake culture tube and AggreWell plate aggregates (Figure 4.1B and Figure 4.2B).

4.1.3 Conformal coating of aggregates generated in AggreWell plates

An alternative method to enhance the shear resistance of aggregates subjected to the higher EDR values encountered during the encapsulation process was tested. Accordingly, the conformal coating method introduced by Dr. Tse and his research group (Kozlovskaya *et al.*, 2012; Pham-Hua *et al.*, 2017) was investigated. This method is a multilayer deposition of hydrogen-bonded poly(N-vinylpyrrolidone), PVPON, and tannic acid (TA) bilayers on the surface of cellular aggregates. In this method, aggregates are first coated by PVPON adsorption on the aggregate surface followed by deposition of the TA. This bilayer deposition of $(PVPON/TA)_n$ can be repeated (here n denotes the number of PVPON/TA bilayers). After aggregates were coated with $(PVPON/TA)_2$ or $(PVPON/TA)_6$, they were analyzed for shear resistance. However, from Figure 4.3 it can be seen that for both conditions 80% of the coated aggregates were damaged within the first 10 minutes. This was lower than the recovery of the uncoated aggregates reported in sections 4.1.1 and 4.1.2. It

may be that the PVPON/TA coating process that requires extensive washing and centrifugation steps contributed to this result.

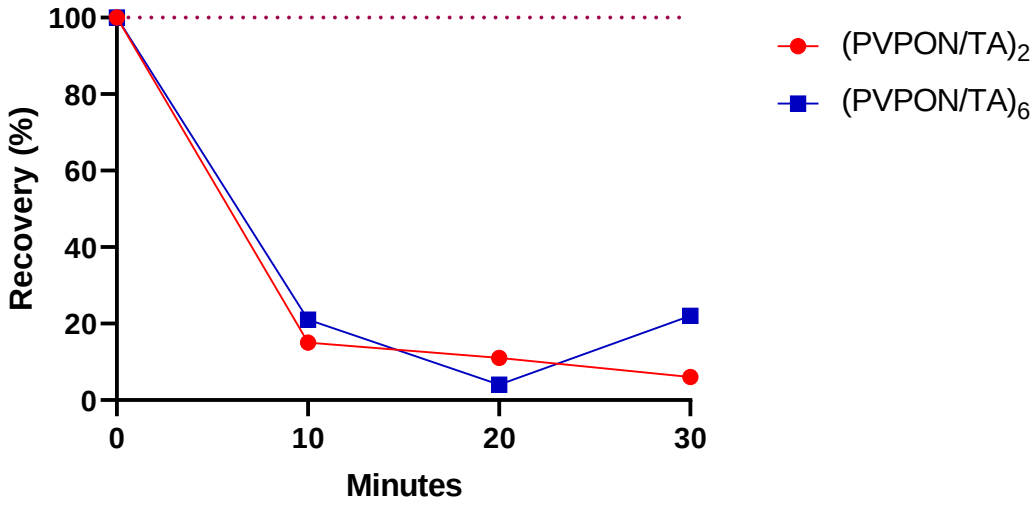

Figure 4.3 Shear resistance of the aggregates coated with (PVPON/TA) bilayers.
Shear resistance experiments conducted using a grid impeller spinner flask at 580 rpm.

Each layer deposition takes 3 minutes and the washing steps between depositions take another 2 minutes. Therefore, leaving cells out of the incubator and subject to repeated centrifugation and resuspension (e.g., aggregates were centrifuged 36 times for the $(PVPON/TA)_6$ deposition) may cause the aggregates to become more vulnerable to shear forces.

4.2 Analysis of Alginate Microcapsules

Two different, 1.5% (w/v) and 5% (w/v), alginate concentration of the microcapsules were compared to investigate their physical properties and the aggregate encapsulation efficiency.

4.2.1 Generation of 1.5% alginate beads

Before the encapsulation of the MIN6 aggregates, the generation of 1.5% alginate beads was optimized by testing several process parameters including the agitation rate, the emulsification time and the paddle versus the grid impeller. The target diameter of the alginate microcapsule was 500 µm, to avoid oxygen limitations that would cause the death of encapsulated cells. After generating alginate beads using either grid or paddle impellers, their mean dimeters D[4,3] and size distributions were analyzed (Figure 4.4).

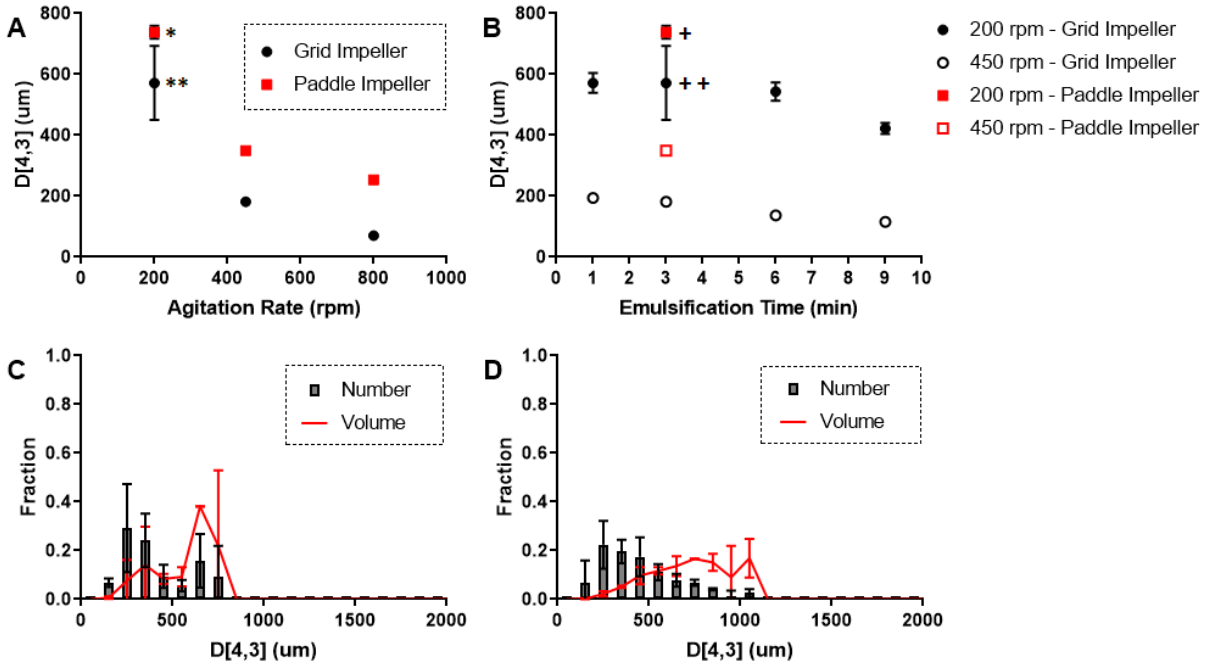

Figure 4.4 Particle size distribution of 1.5% Alginate beads.
(A) The mean and standard deviations of the bead diameter size distribution for a range of agitation rates and 3 minutes emulsification time, *SD=21.4, **SD=121.7. (B) The bead size distributions for a range of emulsification times at the specified agitation rates, +SD=21.3, ++SD=121.7. (C) The histogram of number-weighted and volume weighted alginate bead size distribution generated in the grid impeller spinner flask at 200 rpm for 3 minutes. (D) The histogram of number-weighted and volume weighted alginate bead size distribution generated in the paddle impeller spinner flask at 200 rpm for 3 minutes.

First, with a fixed emulsification time of 3 minutes, different agitation rates were investigated. As seen from Figure 4.4A the alginate beads generated at 200 rpm are closer to the targeted 500 µm diameter. Next, at agitation rates of 200 and 450 rpm, different emulsification times were examined for both the grid and the paddle impeller spinner flasks (Figure 4.4B). The size distributions of the alginate beads generated inside the grid impeller spinner flask at 200 rpm varied around 500 µm, especially for beads emulsified 3 minutes. In Figure 4.4C & D the histograms of alginate beads size distributions for the grid and the paddle impeller spinner flasks at 200 rpm with 3 minutes emulsification time are shown. It was observed that alginate beads generated with the grid impeller had a narrower size distribution compared to the paddle impeller. Therefore, the 1.5% alginate bead generation and encapsulation was performed with a grid impeller spinner flask at 200 rpm with 3 minutes emulsification time. The conditions for 5% alginate bead generation previously established in the lab, 800 rpm and 3 minutes emulsification time, using a gird impeller spinner flask.

4.2.2 Encapsulation efficiency, aspect ratio and size distribution of 1.5% and 5% alginate beads

MIN6 aggregates were encapsulated with 1.5% and 5% alginate solutions to form microcapsules. To reduce the scatter in the data, the encapsulation process was performed 4 times to have biological replicates under the same conditions. The encapsulation products were then sampled for size and encapsulation efficiency analysis. The percent of input cells encapsulated was used as a measure of the encapsulation efficiency (Figure 4.5).

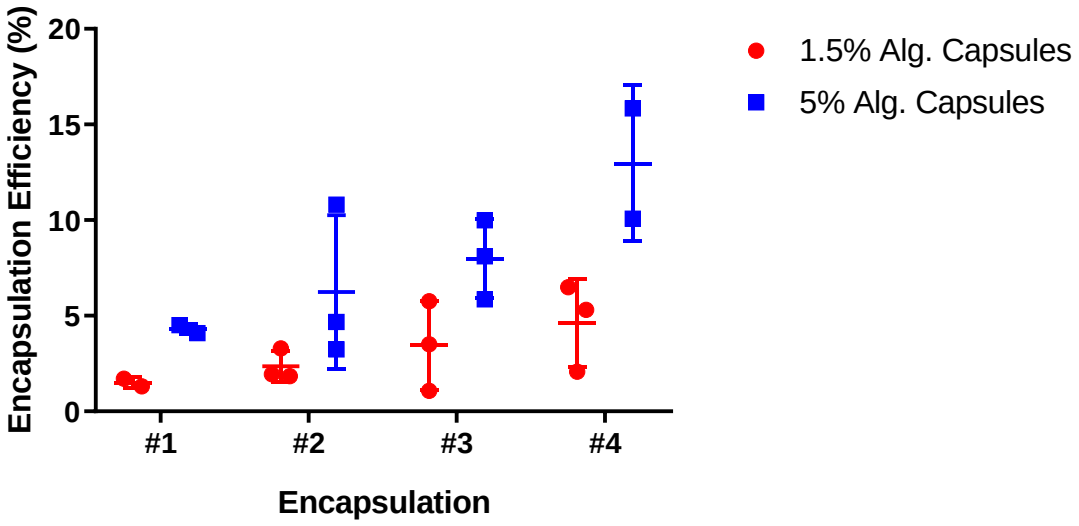

Figure 4.5 Aggregate encapsulation efficiency replicates, comparing 1.5% to 5% alginate microencapsulation.

The overall maximum encapsulation efficiency was only ~15% and for every replicate the mean encapsulation efficiency of the 5% alginate capsules was higher than for the 1.5% alginate capsules.

Many of the 1.5% alginate capsules were observed to have non-spherical, irregular structures. Such non-uniform structure can trigger the inflammatory response as discussed in Chapter 1. Thus, the aspect ratio of the encapsulation product was determined, defined as the ratio of the two perpendicular diameters of a sphere, as a measure of the circularity of the capsules (a circle has an aspect ratio of 1). Although 5% alginate capsules have a narrower distribution, both 1.5% and 5% alginate capsules had mean aspect ratios between 0.9 and 1 (Figure 4.6).

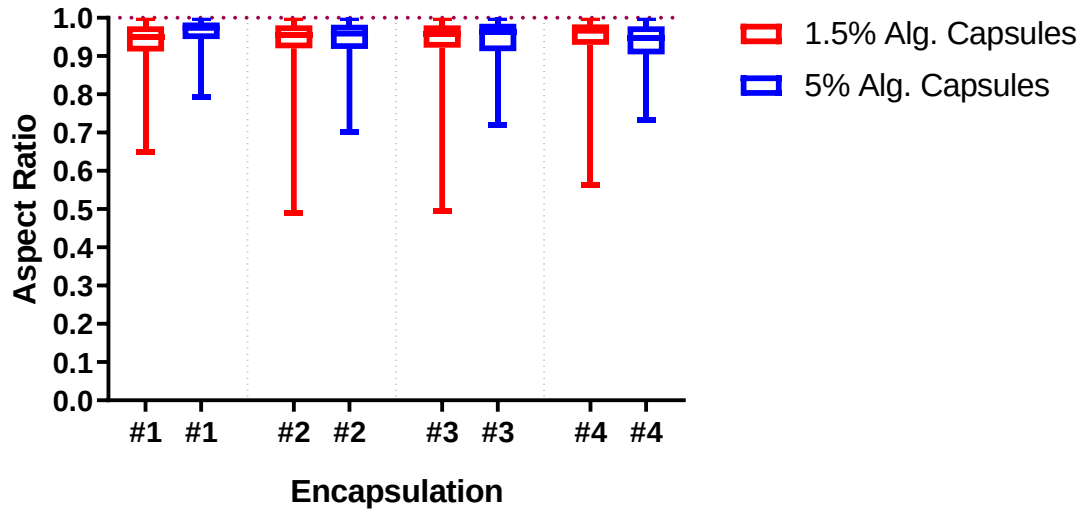

Figure 4.6 Aspect ratios of 1.5% versus 5% alginate capsules.

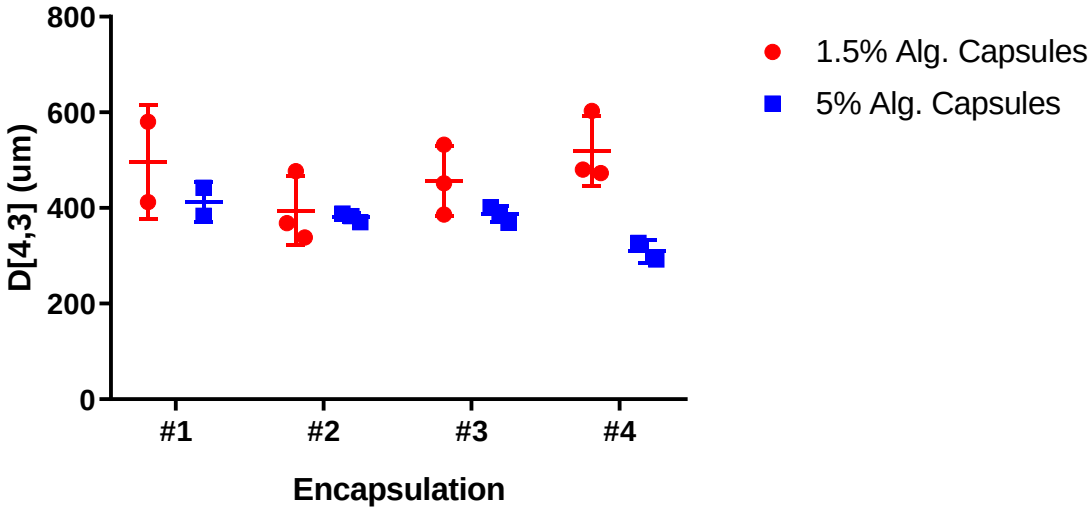

Figure 4.7 Distribution of the alginate capsules diameters.

Narrow size distribution is another desired feature of the encapsulation product because the diffusion rates of insulin and oxygen depend on the capsule diameters. As mentioned in Chapter 1, oxygen availability impacts the viability of encapsulated cells and, upon cell

death, the host immune system reaction. The 5% alginate capsules had a narrower size distribution in all 4 biological replicates with similar D[4,3] mean diameters (Figure 4.7). Considering all these physical features and the encapsulation efficiency results of 1.5% and 5% alginate capsules, the 5% alginate capsules represent a better choice for further scale-up production and application of encapsulation technology.

Chapter 5: Conclusion and Future Work

5.1 Conclusions

Cell aggregation increases the functionality of pancreatic cells due to cell-cell interactions, and aggregation of single cells can be used to generate a model system for islets so as to facilitate the investigation of the impact of bioprocess variables. This study focused on exploring cell aggregation methods and their resistance to shear. The MIN6 β-cell line was used to generate cell aggregates with the target diameter of 150 μm, the average diameter of primary human islets used for diabetes transplantation therapy.

MIN6 cell aggregation was first tested in shaking agitation systems, at 37℃ and 5% CO_2 in humidified incubators. Cell aggregation using an orbital shaker with a 20 mm throw was compared with a Kuhner shaker with a 50 mm throw, at varied agitation rates. It was concluded that 225 rpm in the Kuhner shaker incubator yielded more spherical aggregates with the target diameter of 150 μm. Subsequently, the initial cell input number, the culture time and the medium exchange schedule of the aggregate suspensions were investigated. The results showed no benefit from culturing more than 7 days since the average aggregate diameters did not increase after day 7. However, increasing the medium exchange from every week to every 2 days did increase the aggregate diameters up to the 150 μm target diameter by day 7. Thus, for shaking aggregation, the MIN6 cells were then cultured at 225 rpm in the Kuhner shaker with $0.35x10^6$ cells/mL initial cell input for 7 days with feeding every two days.

A MIN6 cell aggregation method was then developed using AggreWell plates that contain arrays of 400 μm wide microwells with an inverted pyramid structure. This non-shaking aggregation method was adapted to MIN6 cells so as to generate aggregates within 3 days. Besides having the 150 μm target diameter, aggregates generated in AggreWell plates had more uniform spherical structures and narrower size distributions than the aggregates generated in shake tubes. Moreover, approximately the same amount of aggregates generated in shake tubes over 7 days were generated by the AggreWell plates in 3 days. Thus, the AggreWell plates were used to generate aggregates for the subsequent experiments in this study, except for when the shear resistances of the aggregates generated by both methods were compared.

A disaggregation method was then investigated to analyze the cell number and viability of the component cells found in aggregates. For this purpose, varied volumes of TrypLE and incubation time were combined with and without shear force at 225 rpm. Adequate disaggregation was not obtained without shear force (shaking in the incubator). To determine whether the TrypLE reagent may impact the cells viability, single cells were subject to the same process as applied to the aggregates. However, no negative impact of TrypLE was observed. The selected conditions for controllable disaggregation with either 2400 or 4800 aggregates were to use 1 mL TrypLE with 10 minutes incubation at 225 rpm in Kuhner shaker. With these defined conditions, all of the aggregates were disaggregated to healthy single cells.

An aim of this project was to use these MIN6 aggregates as a model system for islet cell encapsulation. Since cells are exposed to high shear forces during the emulsification, it was important to determine the impact of these shear forces on the aggregates. A previously introduced analytical scale, Energy Dissipation Rate (EDR), was used in this study so as to quantify the shear. The recovery of aggregates was high after exposure to low mean EDRs. However, at EDRs of 10^4 W/m^3 (the highest mean level in the encapsulation process) the aggregate recovery was very low. To enhance the shear resistances of aggregates, they were then sequentially treated with poly(N-vinylpyrrolidone), PVPON, and tannic acid (TA) solutions to generate bilayers of PVPON/TA on the surface of the aggregates. Then, they were exposed to shear at 580 rpm agitation rate corresponding to the EDR of $2.5x10^3$ W/m^3 to examine the effect of this coating on the aggregate shear resistances. However, the aggregate recovery results, ~5-20%, were actually lower than the uncoated aggregates that had recovery of ~60% at this EDR of $2.5x10^3$ W/m^3.

The impact of the alginate concentration on the 1.5% (w/v) and 5% (w/v) alginate capsule physical properties was then investigated. Accordingly, the encapsulation efficiency, the aspect ratio of the capsules and their size distribution were analyzed. The operating conditions for the generation of 1.5% alginate beads was first determined as 3 minutes emulsification time at 200 rpm using a grid impeller spinner flask. Then the encapsulation of the generated aggregates with both 1.5% alginate beads and 5% alginate beads were compared using four different replicate experiments. In every replicate the 5% alginate capsules had higher encapsulation efficiency, increased circularity and narrower size distribution than the 1.5% alginate capsules. Even though the encapsulation efficiency for the

5% alginate capsules was higher, the overall efficiency in the final encapsulation product was still low for both 1.5% and 5% alginate capsules.

5.2 Suggestions for Future Work

Cell aggregation with shaking agitation in Kuhner shaker should be tested for different agitation rates. Aggregates generated in shake tube with agitation had higher recovery results after shear exposure than aggregates generated in AggreWell plates, on the other hand AggreWell plate aggregates had more uniform and spherical shape with a narrower size distribution than shake tube aggregates. Thus, to generate more uniform aggregates with a narrower size distribution and at the same time more sturdy against to shear exposure, aggregates should be transferred into shake tube after generation in AggreWell plates and then should be kept culturing for extra one or wo days. This might also help to increase encapsulated aggregate yield if more sturdy aggregates can be generated.

The highest encapsulation efficiency result was only 15%, and this would need to be improved. As some of the losses are likely due to viscosity of the initial alginate solution, the mixing step of aggregate suspensions with alginate solutions could be tested using a tube rotator. Using a tube rotator might provide more gentile mixing than pushing the plunger of a syringe up and down. In addition, the shear resistance of aggregates could be enhanced by different conformal coating methods, to obtain a more robust protection of the aggregates. The shear resistance experiments could be conducted with other cell lines, especially neonatal porcine islets (NPI), since NPI is one of the potential cell sources for

transplantation. Moreover, primary islets or human stem cell derived β cells could be analyzed with the same shear stress system as well.

In the shear resistant experiments, no single cells were observed during image analysis. A possible reason for this observation is that during aggregate recovery measurements, samples were settled under gravity for 10 minutes after shear exposure, so that the recovered aggregates would sediment. Then, 80% of the sample volume was discarded as supernatant and the remainder of the sample was used for image analysis of the recovered aggregates. Thus, to address whether the observed losses in the aggregate numbers are due to either disaggregation of the aggregates into single cells or the lysis of the cells, the supernatant should be imaged and analyzed by the automated cell counter. Furthermore, to address the same issue, the supernatant of aggregate suspensions after shear exposure should also be analyzed by LDH assay whether aggregates are lysed or not.

Besides 1.5% (w/v) and 5% (w/v) alginate microcapsules, other alginate concentrations could be tested to improve the encapsulation efficiency. Since 5% alginate microcapsules had consistently higher encapsulation efficiency than 1.5% alginate microcapsules in every biological replicate, microencapsulation with higher than 5% (w/v) alginate should be investigated for encapsulation efficiency. Furthermore, examination of roughness and surface structure of microcapsules should be investigated to reduce or eliminate the immune reaction.

Bibliography

Andralojc, K. M. *et al.* (2009) 'Ghrelin-producing epsilon cells in the developing and adult human pancreas', *Diabetologia*, 52(3), pp. 486–493. doi: 10.1007/s00125-008-1238-y.

Bassi, R. and Fiorina, P. (2011) 'Impact of islet transplantation on diabetes complications and quality of life', *Current Diabetes Reports*, 11(5), pp. 355–363. doi: 10.1007/s11892-011-0211-1.

Bernard, A. B., Lin, C.-C. and Anseth, K. S. (2012) 'A Microwell Cell Culture Platform for the Aggregation of Pancreatic β-Cells', *Tissue Engineering Part C: Methods*, 18(8), pp. 583–592. doi: 10.1089/ten.tec.2011.0504.

Bieback, K. *et al.* (2009) 'Human alternatives to fetal bovine serum for the expansion of mesenchymal stromal cells from bone marrow', *Stem Cells*, 27(9), pp. 2331–2341. doi: 10.1002/stem.139.

Brereton, M. F. *et al.* (2015) 'Alpha-, Delta- and PP-cells: Are They the Architectural Cornerstones of Islet Structure and Co-ordination?', *Journal of Histochemistry and Cytochemistry*, 63(8), pp. 575–591. doi: 10.1369/0022155415583535.

Brissova, M. *et al.* (2005) 'Assessment of human pancreatic islet architecture and composition by laser scanning confocal microscopy', *Journal of Histochemistry and Cytochemistry*, 53(9), pp. 1087–1097. doi: 10.1369/jhc.5C6684.2005.

Buchwald, P. *et al.* (2009) 'Quantitative assessment of islet cell products: Estimating the

accuracy of the existing protocol and accounting for islet size distribution', *Cell Transplantation*, 18(10–11), pp. 1223–1235. doi: 10.3727/096368909X476968.

Burridge, P. W. *et al.* (2007) 'Improved Human Embryonic Stem Cell Embryoid Body Homogeneity and Cardiomyocyte Differentiation from a Novel V-96 Plate Aggregation System Highlights Interline Variability', *Stem Cells*, 25(4), pp. 929–938. doi: 10.1634/stemcells.2006-0598.

Cabrera, O. *et al.* (2006) 'The unique cytoarchitecture of human pancreatic islets has implications for islet cell function', *Proceedings of the National Academy of Sciences*, 103(7), pp. 2334–2339. doi: 10.1073/pnas.0510790103.

Calafiore, R. *et al.* (2006) 'Microencapsulated Pancreatic Islet Allografts Into Nonimmunosuppressed Patients With Type 1 Diabetes', *Diabetes Care*, 29(1), pp. 137–138.

Calafiore, R. *et al.* (2006) 'Standard Technical Procedures for Microencapsulation of Human Islets for Graft into Nonimmunosuppressed Patients With Type 1 Diabetes Mellitus', *Transplantation Proceedings*, 38(4), pp. 1156–1157. doi: 10.1016/j.transproceed.2006.03.014.

Canadian Diabetes Association (no date) *Diabetes Statistics in Canada*. Available at: http://www.diabetes.ca/how-you-can-help/advocate/why-federal-leadership-is-essential/diabetes-statistics-in-canada (Accessed: 8 June 2018).

Chatterjee, S., Khunti, K. and Davies, M. J. (2017) 'Type 2 diabetes', *The Lancet*. Elsevier Ltd, 389(10085), pp. 2239–2251. doi: 10.1016/S0140-6736(17)30058-2.

Dang, S. M. *et al.* (2002) 'Efficiency of embryoid body formation and hematopoietic development from embryonic stem cells in different culture systems', *Biotechnology and Bioengineering*, 78(4), pp. 442–453. doi: 10.1002/bit.10220.

Desai, T. and Shea, L. D. (2017) 'Advances in islet encapsulation technologies', *Nature Reviews Drug Discovery*. Nature Publishing Group, 16(5), pp. 338–350. doi: 10.1038/nrd.2016.232.

Donath, M. Y. and Shoelson, S. E. (2011) 'Type 2 Diabetes as an inflammatory disease', *Nature Reviews Immunology*, 11(2), pp. 98–107. Available at: http://www.bibliotecarazetti.com/Articulos/diabetes tipo 2 como una enfermedad inflamatoria.pdf.

Elliott, R. B. *et al.* (2007) 'Live encapsulated porcine islets from a type 1 diabetic patient 9.5 yr after xenotransplantation', *Xenotransplantation*, 14(2), pp. 157–161. doi: 10.1111/j.1399-3089.2007.00384.x.

Ertesvåg, H. and Valla, S. (1998) 'Biosynthesis and applications of alginates', *Polymer Degradation and Stability*, 59(1–3), pp. 85–91. doi: 10.1016/S0141-3910(97)00179-1.

Furukawa, H. *et al.* (2012) 'Correlation of power consumption for several kinds of mixing impellers', *International Journal of Chemical Engineering*, 2012, pp. 1–6. doi: 10.1155/2012/106496.

Gilbertson, J. A. *et al.* (2006) 'Scaled-up production of mammalian neural precursor cell aggregates in computer-controlled suspension bioreactors', *Biotechnology and*

Bioengineering, 94(4), pp. 783–792. Available at: https://onlinelibrary-wiley-com.ezproxy.library.ubc.ca/doi/abs/10.1002/bit.20900.

Goh, C. H., Heng, P. W. S. and Chan, L. W. (2012) 'Alginates as a useful natural polymer for microencapsulation and therapeutic applications', *Carbohydrate Polymers*. Elsevier Ltd., 88(1), pp. 1–12. doi: 10.1016/j.carbpol.2011.11.012.

Gregoriades, N. *et al.* (2000) 'Cell Damage of Microcarrier Cultures as a Function of Local Energy Dissipation Created by a Rapid Extensional Flow', *Biotechnology and Bioengineering*, 69(2), pp. 171–182.

Hauge-Evans, A. C. *et al.* (1999) 'Pancreatic β-cell-to-β-cell interactions are required for integrated responses to nutrient stimuli: Enhanced Ca2+ and insulin secretory responses of MIN6 pseudoislets', *Diabetes*, 48(7), pp. 1402–1408. doi: 10.2337/diabetes.48.7.1402.

Hilderink, J. *et al.* (2015) 'Controlled aggregation of primary human pancreatic islet cells leads to glucose-responsive pseudoislets comparable to native islets', *Journal of Cellular and Molecular Medicine*, 19(8), pp. 1836–1846. doi: 10.1111/jcmm.12555.

Hoesli, C. (2010) *Bioprocess Development for the Cell-Based Treatment of Diabetes*. University of British Columbia.

Hoesli, C. A. *et al.* (2011) 'Pancreatic cell immobilization in alginate beads produced by emulsion and internal gelation', *Biotechnology and Bioengineering*, 108(2), pp. 424–434. doi: 10.1002/bit.22959.

Hoesli, C. A. *et al.* (2012) 'Reversal of diabetes by βTC3 cells encapsulated in alginate beads

generated by emulsion and internal gelation', *Journal of Biomedical Materials Research - Part B*, 100B(4), pp. 1017–1028. doi: 10.1002/jbm.b.32667.

Huang, H. H., Ramachandran, K. and Stehno-Bittel, L. (2013) 'A replacement for islet equivalents with improved reliability and validity', *Acta Diabetologica*, 50(5), pp. 687–696. doi: 10.1007/s00592-012-0375-4.

International Diabetes Federation (2017) *IDF Diabetes Atlas*, *Public Policy Analysis*. doi: 10.1016/B978-0-08-044382-9.50032-7.

Ishihara, H. *et al.* (1993) 'Pancreatic beta cell line MIN6 exhibits characteristics of glucose metabolism and glucose-stimulated insulin secretion similar to those of normal islets', *Diabetologia*, 36(11), pp. 1139–1145. doi: 10.1007/BF00401058.

Johannesson, B. *et al.* (2015) 'Toward beta cell replacement for diabetes.', *The EMBO journal*, 34(7), pp. 841–55. doi: 10.15252/embj.201490685.

Jung, Y. S. *et al.* (2012) 'Surface modification of pancreatic islets using heparin-DOPA conjugate and anti-CD154 mAb for the prolonged survival of intrahepatic transplanted islets in a xenograft model', *Biomaterials*. Elsevier Ltd, 33(1), pp. 295–303. doi: 10.1016/j.biomaterials.2011.09.051.

Kelly, C. *et al.* (2010) 'Comparison of Insulin Release From MIN6 Pseudoislets and Pancreatic Islets of Langerhans Reveals Importance of Homotypic Cell Interactions', *Pancreas*, 39(7), pp. 1016–1023.

Kieffer, T. J. *et al.* (2018) 'Beta-cell replacement strategies for diabetes', *Journal of Diabetes*

Investigation, 9(3), pp. 457–463. doi: 10.1111/jdi.12758.

Kizilel, S. *et al.* (2010) 'Encapsulation of pancreatic islets within nano-thin functional polyethylene glycol coatings for enhanced insulin secretion', *Tissue Engineering: Part A*, 16(7), pp. 2217–2228.

Koike, M., Kurosawa, H. and Amano, Y. (2005) 'A round-bottom 96-well polystyrene plate coated with 2-methacryloyloxyethyl phosphorylcholine as an effective tool for embryoid body formation', *Cytotechnology*, 47(1–3), pp. 3–10. doi: 10.1007/s10616-005-3743-x.

Kozlovskaya, V. *et al.* (2012) 'Ultrathin polymeric coatings based on hydrogen-bonded polyphenol for protection of pancreatic islet cells', *Advanced Functional Materials*, 22(16), pp. 3389–3398. doi: 10.1002/adfm.201200138.

Langlois, G. *et al.* (2009) 'Direct effect of alginate purification on the survival of islets immobilized in alginate-based microcapsules', *Acta Biomaterialia*, 5(9), pp. 3433–3440. doi: 10.1016/j.actbio.2009.05.029.

Lee, K. Y. and Mooney, D. J. (2012) 'Alginate: Properties and biomedical applications', *Progress in Polymer Science (Oxford)*. Elsevier Ltd, 37(1), pp. 106–126. doi: 10.1016/j.progpolymsci.2011.06.003.

Lim, F. and Sun, A. M. (1980) 'Microencapsulated Islets as Bioartificial Endocrine Pancreas', *Science*, 210(4472), pp. 908–910.

MacGregor, R. R. *et al.* (2006) 'Small rat islets are superior to large islets in in vitro function and in transplantation outcomes.', *American Journal of Physiology Endocrinology and*

Metabolism, 290(5), pp. E771-779. doi: 10.1152/ajpendo.00097.2005.

Marciniak, A. *et al.* (2014) 'Using pancreas tissue slices for in situ studies of islet of Langerhans and acinar cell biology', *Nature Protocols*, 9(12), pp. 2809–2822. doi: 10.1038/nprot.2014.195.

McAndrews, J. and Wu, J. (2013) 'Introduction to the endocrine system part 2: Physiology', *AMWA Journal*, 28(2), pp. 51–56.

Miyazaki, J. *et al.* (1990) 'Establishment of a Pancreatic β Cell Line That Retains Glucose-Inducible Insulin Secretion : Special Reference to Expression of Glucose Transporter Isoforms *', *Endocrinology*, 127(1), pp. 126–132.

Mollet, M. *et al.* (2004) 'Bioprocess Equipment : Characterization of Energy Dissipation Rate and Its Potential to Damage Cells', *Biotechnology Progress*, 20(5), pp. 1437–1448.

Murua, A. *et al.* (2011) 'Design of a composite drug delivery system to prolong functionality of cell-based scaffolds', *International Journal of Pharmaceutics*. Elsevier B.V., 407(1–2), pp. 142–150. doi: 10.1016/j.ijpharm.2010.11.022.

Paredes-Juarez, G. A. *et al.* (2015) 'DAMP production by human islets under low oxygen and nutrients in the presence or absence of an immunoisolating-capsule and necrostatin-1', *Scientific Reports*. Nature Publishing Group, 5(September), pp. 1–12. doi: 10.1038/srep14623.

Paredes Juarez, G. A. *et al.* (2014) 'Immunological and Technical Considerations in Application of Alginate-Based Microencapsulation Systems', *Frontiers in Bioengineering*

and Biotechnology, 2(August), pp. 1–15. doi: 10.3389/fbioe.2014.00026.

Pham-Hua, D. *et al.* (2017) 'Islet encapsulation with polyphenol coatings decreases pro-inflammatory chemokine synthesis and T cell trafficking', *Biomaterials*. Elsevier Ltd, 128, pp. 19–32. doi: 10.1016/j.biomaterials.2017.03.002.

Poncelet, D. *et al.* (1992) 'Production of alginate beads by emulsification/internal gelation. I. Methodology', *Applied Microbiology and Biotechnology*, 38(1), pp. 39–45. doi: 10.1007/BF00164768.

Robertson, R. P. (2004) 'Islet transplantation as a treatment for diabetes - a work in progress', *N.Engl.J.Med.*, 350(7), pp. 694–705.

Ryan, E. A. *et al.* (2005) 'Five year follow-up after clinical islet transplantation', *Diabetes*, 54(7), pp. 2060–2069.

Sakai, S. *et al.* (2004) 'MIN6 cells-enclosing aminopropyl-silicate membrane templated by alginate gels differences in guluronic acid content', *International Journal of Pharmaceutics*, 270(1–2), pp. 65–73. doi: 10.1016/j.ijpharm.2003.10.014.

Scharp, D. W. and Marchetti, P. (2014) 'Encapsulated islets for diabetes therapy: History, current progress, and critical issues requiring solution', *Advanced Drug Delivery Reviews*. Elsevier B.V., 67–68, pp. 35–73. doi: 10.1016/j.addr.2013.07.018.

Schulz, T. C. *et al.* (2012) 'A scalable system for production of functional pancreatic progenitors from human embryonic stem cells', *PLoS ONE*, 7(5), p. e37004. doi: 10.1371/journal.pone.0037004.

Sen, A., Kallos, M. S. and Behie, L. A. (2001) 'Effects of hydrodynamics on cultures of mammalian neural stem cell aggregates in suspension bioreactors', *Industrial and Engineering Chemistry Research,* 40(23), pp. 5350–5357. doi: 10.1021/ie001107y.

Shapiro, A. M. J. *et al.* (2000) 'Islet Transplantation in Seven Patients with Type 1 Diabetes Mellitus Using a Glucocorticoid-Free Immunosuppressive Regimen', *The New England Journal of Medicine,* 343(4), pp. 230–238. doi: 10.1056/NEJM200007273430401.

Shapiro, A. M. J. *et al.* (2006) 'International Trial of the Edmonton Protocol for Islet Transplantation', *New England Journal of Medicine*, 355(13), pp. 1318–1330. doi: 10.1056/NEJMoa061267.

Shenkman, R. M. *et al.* (2009) 'Effects of energy dissipation rate on islets of langerhans: Implications for isolation and transplantation', *Biotechnology and Bioengineering*, 103(2), pp. 413–423. doi: 10.1002/bit.22241.

Skelin, M., Rupnik, M. and Cencic, A. (2010) 'Pancreatic beta cell lines and their applications in diabetes mellitus research.', *Altex*, 27(2), pp. 105–113. doi: 10.14573/altex.2010.2.105.

Song, S. and Roy, S. (2016) 'Progress and challenges in macroencapsulation approaches for type 1 diabetes (T1D) treatment: Cells, biomaterials, and devices', *Biotechnology and Bioengineering*, 113(7), pp. 1381–1402. doi: 10.1002/bit.25895.

Ungrin, M. D. *et al.* (2008) 'Reproducible, ultra high-throughput formation of multicellular organization from single cell suspension-derived human embryonic stem cell aggregates',

PLoS ONE, 3(2). doi: 10.1371/journal.pone.0001565.

Ungrin, M. D. *et al.* (2012) 'Rational bioprocess design for human pluripotent stem cell expansion and endoderm differentiation based on cellular dynamics', *Biotechnology and Bioengineering*, 109(4), pp. 853–866. doi: 10.1002/bit.24375.

Vaithilingam, V. and Tuch, B. E. (2011) 'Islet Transplantation and Encapsulation : An Update on Recent Developments', *The Review of Diabetic Studies*, 8(1), pp. 51–67. doi: 10.1900/RDS.2011.8.51.

Verbridge, S. S., Chandler, E. M. and Fischbach, C. (2010) 'Tissue-Engineered Three Dimensional Tumor Models to Study Tumor Angiogenesis', *Tissue Engineering: Part A*, 16(7), pp. 2147–2152.

Vlahos, A. E., Cober, N. and Sefton, M. V. (2017) 'Modular tissue engineering for the vascularization of subcutaneously transplanted pancreatic islets', *Proceedings of the National Academy of Sciences*, 114(35), p. 201619216. doi: 10.1073/pnas.1619216114.

de Vos, P. *et al.* (2003) 'Association between macrophage activation and function of micro-encapsulated rat islets', *Diabetologia*, 46(5), pp. 666–673. doi: 10.1007/s00125-003-1087-7.

de Vos, P. *et al.* (2006) 'Alginate-based microcapsules for immunoisolation of pancreatic islets', *Biomaterials*, 27(32), pp. 5603–5617. doi: 10.1016/j.biomaterials.2006.07.010.

De Vos, P. *et al.* (1997) 'Improved biocompatibility but limited graft survival after purification of alginate for microencapsulation of pancreatic islets', *Diabetologia*, 40(3), pp. 262–270. doi: 10.1007/s001250050673.

De Vos, P. *et al.* (1999) ‘Why do microencapsulated islet grafts fail in the absence of fibrotic overgrowth?’, *Diabetes*, 48(7), pp. 1381–1388. doi: 10.2337/diabetes.48.7.1381.

De Vos, P. *et al.* (2014) ‘Polymers in cell encapsulation from an enveloped cell perspective’, *Advanced Drug Delivery Reviews*. Elsevier B.V., 67–68, pp. 15–34. doi: 10.1016/j.addr.2013.11.005.

De Vos, P., Hamel, A. F. and Tatarkiewicz, K. (2002) ‘Considerations for successful transplantation of encapsulated pancreatic islets’, *Diabetologia*, 45(2), pp. 159–173. doi: 10.1007/s00125-001-0729-x.

Wallner, K. *et al.* (2018) ‘Stem cells and beta cell replacement therapy: A prospective health technology assessment study’, *BMC Endocrine Disorders*. BMC Endocrine Disorders, 18(1), pp. 1–12. doi: 10.1186/s12902-018-0233-7.

Wardle, J. (2013) ‘Type I diabetes: pancreas and islet transplantation’, *Practice Nursing*, 24(5), pp. 243–246.

WHO (2014) *Global report on diabetes., World Health Organization*. doi: 10.1128/AAC.03728-14.

Yamada, K. M. and Cukierman, E. (2007) ‘Modeling Tissue Morphogenesis and Cancer in 3D’, *Cell*, 130(4), pp. 601–610. doi: 10.1016/j.cell.2007.08.006.

Yang, K.-C. *et al.* (2013) ‘Investigating the suspension culture on aggregation and function of mouse pancreatic β-cells’, *Journal of Biomedical Materials Research Part A*, 101A(8), pp. 2273–2282. doi: 10.1002/jbm.a.34547.

Youn, B. S. *et al.* (2005) 'Large-scale expansion of mammary epithelial stem cell aggregates in suspension bioreactors', *Biotechnology Progress*, 21(3), pp. 984–993. doi: 10.1021/bp050059f.

Youn, B. S. *et al.* (2006) 'Scale-up of breast cancer stem cell aggregate cultures to suspension bioreactors', *Biotechnology Progress*, 22(3), pp. 801–810. doi: 10.1021/bp050430z.

Zhi, Z. L. *et al.* (2010) 'Polysaccharide multilayer nanoencapsulation of insulin-producing β-cells grown as pseudoislets for potential cellular delivery of insulin', *Biomacromolecules*, 11(3), pp. 610–616. doi: 10.1021/bm901152k.

Zimmermann, H. *et al.* (2005) 'Towards a medically approved technology for alginate-based microcapsules allowing long-term immunoisolated transplantation', *Jounal of Materials Science: Materials in Medicine*, 16(6), pp. 491–501.

Zinger, A. and Leibowitz, G. (2014) 'Islet Transplantation in Type 1 Diabetes: hype, hope and reality - a clinician's perspective', *Diabetes/Metabolism Research and Reviews*, 30(2), pp. 83–87. doi: 10.1002/dmrr.

Appendices

Appendix A Supplementary data

A.1 Cellular growth curve of MIN6 cells

To show the cellular growth of the MIN6 cells over 7 days, seven different T75-Flask were set up with the same initial cell input ($0.05x10^6$ cells/cm^2) and cell enumeration was performed by Cedex on each day.

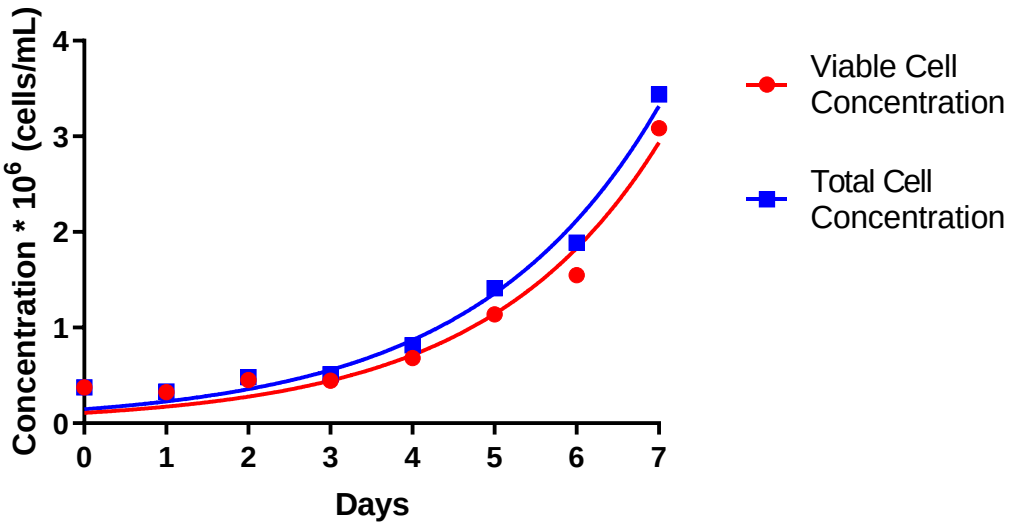

Figure A.1 Growth of MIN6 cells in a T-Flask.

A.2 Estimation of the power number of the paddle impeller

The correlation equations of power consumption of paddle impeller suggested by Furukawa *et al.* (2012) was used to estimate impeller power number. For this estimation some assumptions were made. First, the paddle impeller assumed to have two blades because the stir bar edges might act as smaller blades and the suggested impeller power number correlations take into accounts only geometrically identical impeller blades. Second, as also mentioned in Section 4.1 when the highest agitation rate is reached, the spinner flask is partially filled with 30-40 mL mineral oil. Since there is no impeller power number correlations for partially filled vessels, the spinner flask was assumed to be filled with 100 mL mineral oil during whole process. With this assumptions, the impeller power number (N_p):

$$N_p = \left[\frac{1.2\pi^4\beta^2}{8\left(\frac{d^3}{D^2H}\right)}\right] f \qquad \textbf{Equation A.1}$$

Where β is geometric parameter defined by:

$$\beta = \frac{2ln\left(\frac{D}{d}\right)}{\left(\frac{D}{d}\right)-\left(\frac{d}{D}\right)} \qquad \textbf{Equation A.2}$$

And f is the friction factor defined by:

$$f = \frac{C_L}{Re_G} + C_t\left[\left(\frac{C_{tr}}{Re_G} + Re_G\right)^{-1} + \left(\frac{f_\infty}{C_t}\right)^{\frac{1}{m}}\right]^m \qquad \textbf{Equation A.3}$$

Where Re_G is a modified Reynolds number, f_∞ is the asymptotic value of f when $Re_G \to \infty$ and C_L, C_{tr}, and C_t are empirical coefficients. These are defined by the equations as follows:

$$Re_G = \left[\frac{\pi\eta\beta D}{4d} ln\left(\frac{D}{d}\right)\right] Re_d$$ **Equation A.4**

$$Re_d = \frac{Nd^2\rho}{\mu}$$ **Equation A.5**

$$C_L = 0.215\eta n_b \left(\frac{d}{H}\right)\left[1 - \left(\frac{d}{D}\right)^2\right] + 1.83\left(\frac{bsin\theta}{H}\right)\left(\frac{n_b}{2sin\theta}\right)^{\frac{1}{3}}$$ **Equation A.6**

$$C_t = \left\{\left[1.96\left(\frac{\gamma n_b^{0.7} b}{D}\right)^{1.19}\right]^{-7.8} + (0.25)^{-7.8}\right\}^{-\frac{1}{7.8}}$$ **Equation A.7**

$$C_{tr} = 23.8\left(\frac{d}{D}\right)^{-3.24}\left(\frac{bsin\theta}{D}\right)^{-1.18} X^{-0.74}$$ **Equation A.8**

$$f_\infty = 0.0151\left(\frac{d}{D}\right) C_t^{0.308}$$ **Equation A.9**

$$m = [(0.710X^{0.373})^{-7.8} + (0.333)^{-7.8}]^{-\frac{1}{7.8}}$$ **Equation A.10**

$$X = \frac{\gamma n_b^{0.7} sin^{1.6}\theta}{H}$$ **Equation A.11**

$$\gamma = \left[\frac{\eta ln\left(\frac{D}{d}\right)}{\left(\frac{\beta D}{d}\right)^5}\right]^{\frac{1}{3}}$$ **Equation A.12**

$$\eta = \frac{0.711\left\{0.157 + \left[n_b ln\left(\frac{D}{d}\right)\right]^{0.611}\right\}}{n_b^{0.52}\left[1 - \left(\frac{d}{D}\right)^2\right]}$$ **Equation A.13**

Considering the dimensions of paddle impeller spinner flask (Table 4.1) and the physical properties of mineral oil (Table 4.2) for an agitation rate of 16.7 s^{-1} (1000 rpm) the impeller power number (N_p) and the other correlation values were estimated by the equations given above:

$$N_p = 8.9 \times 10^{-1}$$

$\beta = 9.6 \times 10^{-1}$ $f = 5.7 \times 10^{-2}$

$Re_G = 1.6 \times 10^{2}$ $Re_d = 1.0 \times 10^{3}$

$C_L = 1.7$ $C_t = 2.5 \times 10^{-1}$

$C_{tr} = 1.3 \times 10^{2}$ $f_\infty = 8.5 \times 10^{-3}$

$m = 3.3 \times 10^{-1}$ $X = 7.3 \times 10^{-1}$

$\gamma = 4.4 \times 10^{-1}$ $\eta = 1.2$

Similarly, for the shear resistance experiments using the same vessel dimensions, the physical properties of water and the assumption for the spinner flask filled with 30 mL the same estimations were done to determine the impeller power number and hence the mean EDR values given in Table 4.4.

A.3 Effects of shear forces generated using a grid impeller spinner flask on aggregates

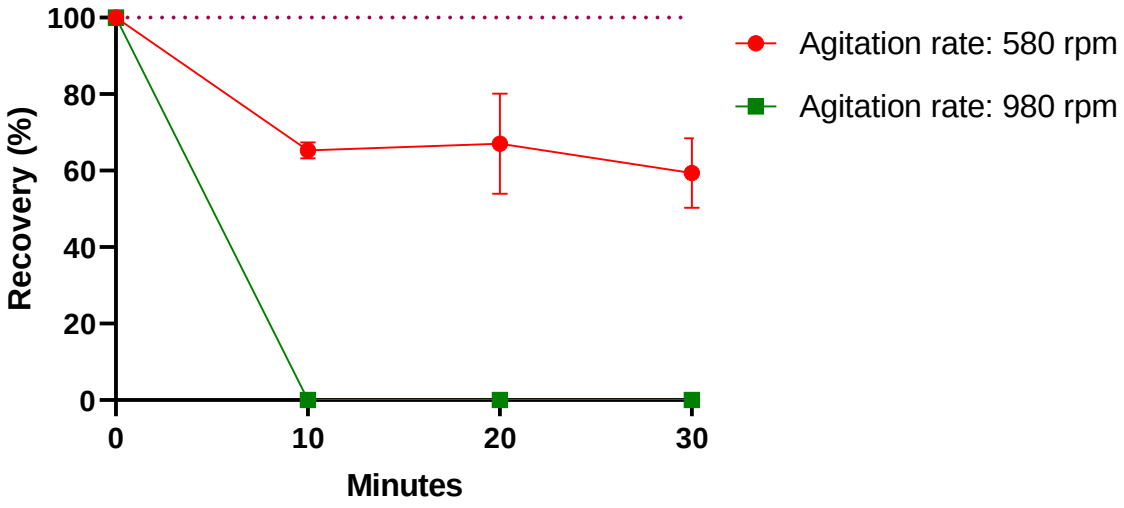

Figure A.2 Shake tube aggregates recovery after exposure to shear stress in a grid impeller spinner flask (n=2).

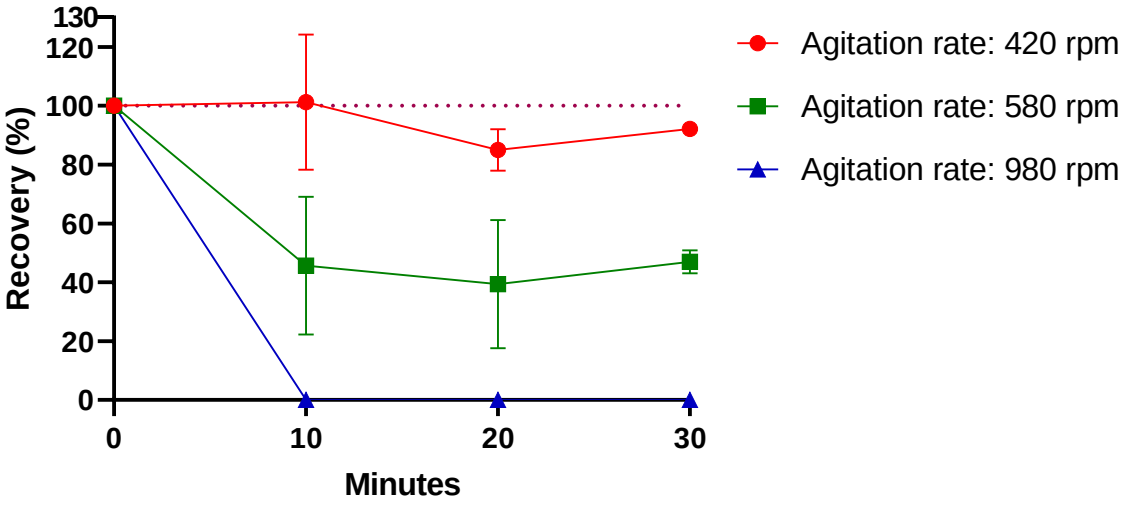

Figure A.3 AggreWell plate aggregates recovery after exposure to shear stress in a grid impeller spinner flask (n=2).

Appendix B Supplementary figures

B.1 Images of aggregates using an orbital shaker

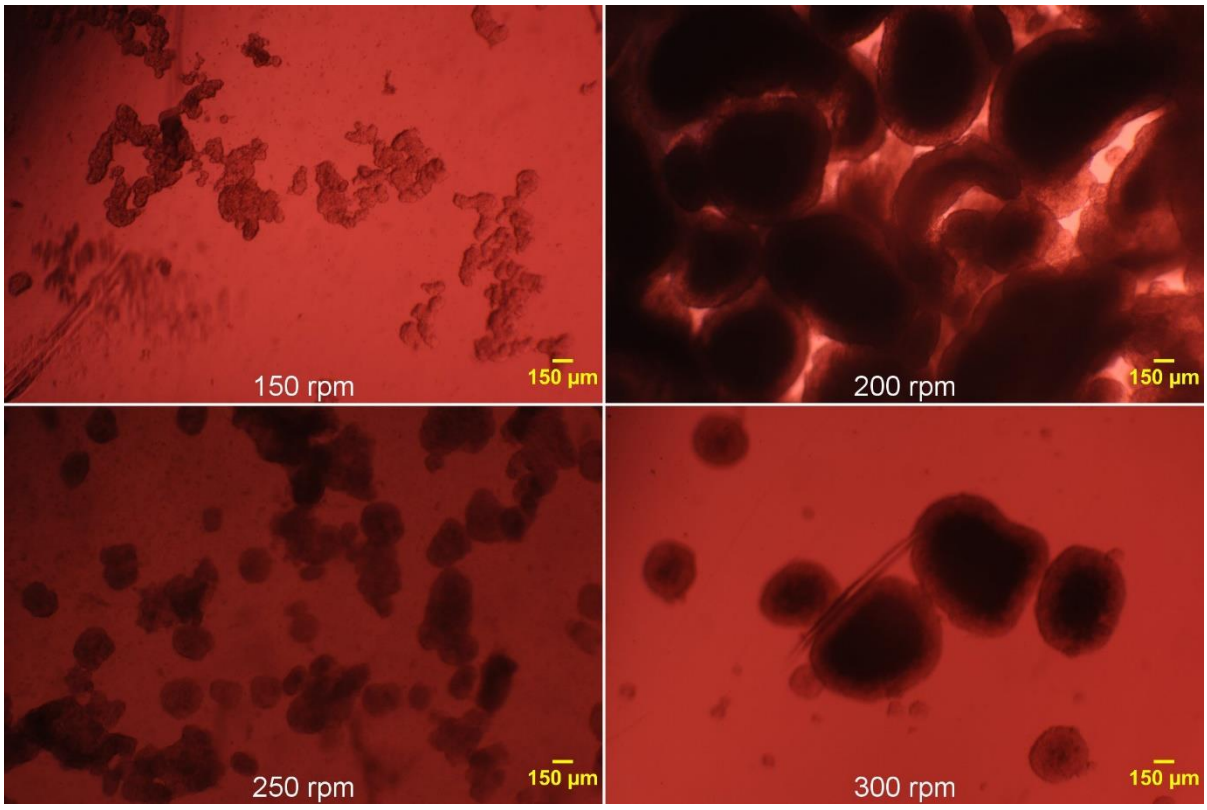

Figure B.1 Aggregation using orbital shaker on day 7 at different agitation rates.
Aggregate generation was failed using orbital shaker because as seen from the figure many of the aggregates have irregular shape. Some of them were much greater than the target diameter whereas others were much smaller. In many of the condition, aggregates were usually settled at the bottom, especially at 150 rpm and 300 rpm. The rest of them suspended in the media did not have the desired uniform spherical aggregate structure.

B.2 Spinner flasks and impeller geometry

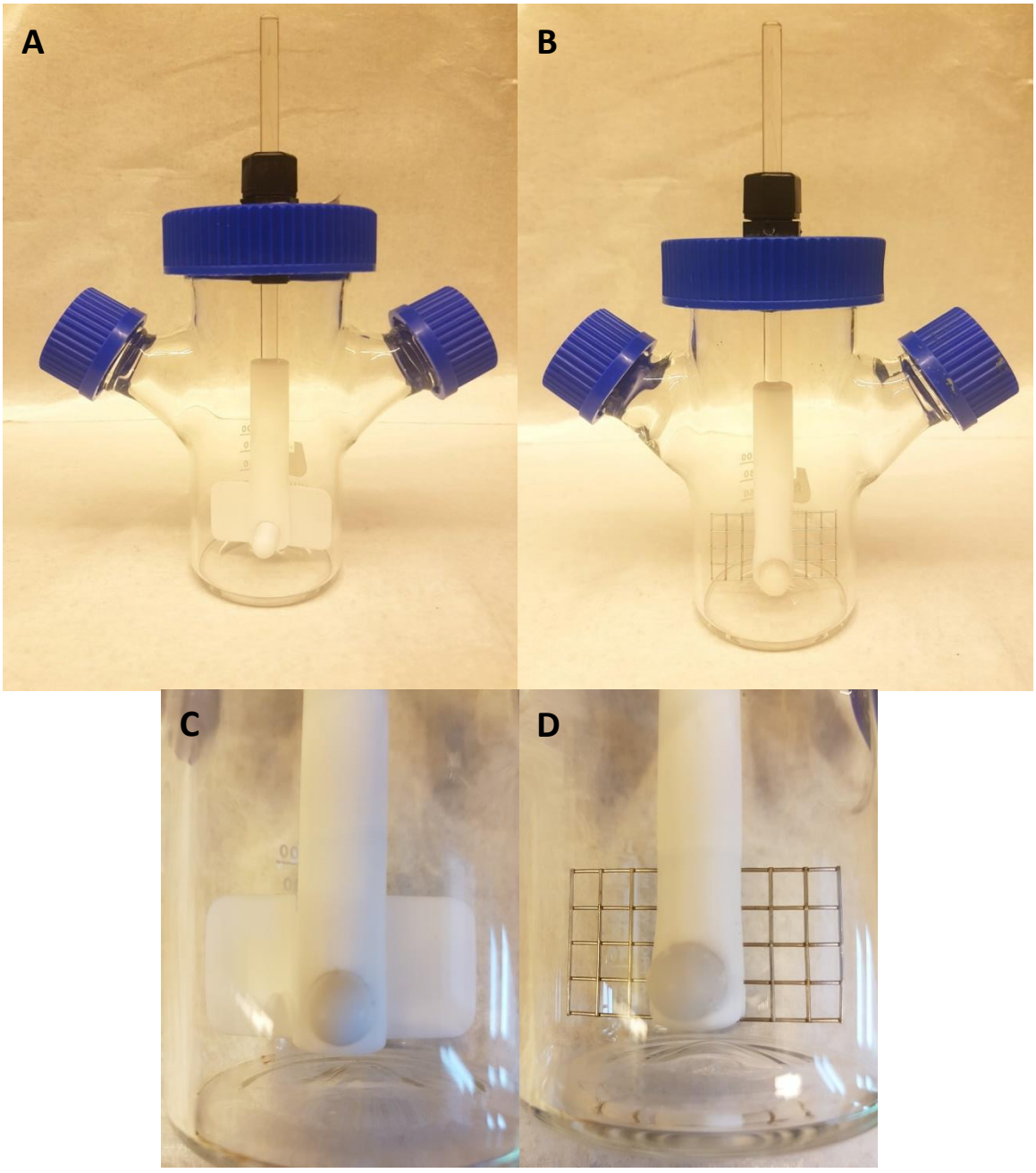

Figure B.2 Paddle impeller and grid impeller spinner flask.
(A) Paddle spinner flask. (B) Grid impeller spinner flask. (C) Paddle impeller geometry. (D) Grid impeller wired lattice geometry.